Functional connectivity differences in Alzheimer's disease and amnestic mild cognitive impairment associated with AT(N) classification and anosognosia

Jaime D. Mondragón [a,b,*], Natasha M. Maurits [a,b], Peter P. De Deyn [a,b,c], for the Alzheimer's Disease Neuroimaging Initiative

[a] University of Groningen, University Medical Center Groningen, Department of Neurology, Groningen, the Netherlands
[b] University of Groningen, University Medical Center Groningen, Alzheimer Center Groningen, Groningen, the Netherlands
[c] Laboratory of Neurochemistry and Behavior, Institute Born-Bunge, University of Antwerp, Antwerp, Belgium

ARTICLE INFO

ABSTRACT

Alzheimer's continuum biological profiles ($A^+T^-N^-$, $A^+T^+N^-$, $A^+T^-N^+$, and $A^+T^+N^+$) were established in the 2018 National Institute on Aging and Alzheimer's Association research framework for Alzheimer's disease (AD). We aim to assess the relation between AT(N) biomarker profiles and brain functional connectivity (FC) and assess the neural correlates of anosognosia. We assessed local functional coupling and between-network connectivity through between-group intrinsic local correlation and independent component analyses. The neural correlates of anosognosia were assessed via voxel-wise linear regression analysis in prodromal AD. Statistical significance for the FC analysis was set at $p \leq 0.05$ false discovery rate (FDR)-corrected for cluster size. One hundred and twenty-one and 73 participants were included in the FC and the anosognosia analysis, respectively. The FC in the default mode network is greater in prodromal AD than AD with dementia (i.e., local correlation: T = 8.26, p-FDR < 0.001, k = 1179; independent component analysis: cerebellar network, T = 4.01, p-FDR = 0.0012, k = 493). The default mode network is persistently affected in the early stages of Alzheimer's biological continuum. The anterior cingulate cortex (T = 2.52, p-FDR = 0.043, k = 704) is associated with anosognosia in prodromal AD.
© 2021 The Author(s). Published by Elsevier Inc. This is an open access article under the CC BY license (http://creativecommons.org/licenses/by/4.0/).

1. Background

The Alzheimer's disease (AD) continuum is both clinical and biological. First, the cognitive decline continuum associated with AD is clinically divided into a preclinical, a prodromal, and a clinical stage (Sperling et al., 2011). Second, the AD biological continuum has been recently defined. In 2018, the research framework for a biological in vivo classification (i.e., AT(N) classification) of AD was published (Jack et al., 2018). Three main groups can be derived from the National Institute on Aging and Alzheimer's Association (NIA-AA) research framework: (1) participants with Alzheimer's pathologic change; (2) participants with non-AD pathologic changes; and (3) participants with normal biomarkers (Jack et al., 2018). The AT(N) system classification allows for a biologically centered definition of AD (Jack et al., 2018). Altogether, beta-amyloid (Aβ) burden (i.e., the "A" in the AT(N) classification system) is the characteristic feature of the Alzheimer's continuum biological profiles (i.e., $A^+T^-N^-$, $A^+T^+N^-$, $A^+T^-N^+$, and $A^+T^+N^+$). Fig. 1 displays the NIA-AA research framework', which divides the 3 AT(N) biomarker types into different biomarker profiles (Jack et al., 2018).

The AT(N) classification permits the stratification into 3 groups within the Alzheimer's biological continuum that are associated with short-term clinical progression: preclinical AD, AD with mild cognitive impairment (MCI) or prodromal AD and AD with dementia (Jack et al., 2018). Importantly for clinical use, Aβ burden can be assessed through cerebrospinal fluid (CSF) amyloid and amyloid positron emission tomography (PET) biomarkers. Amyloid PET is a

		Cognitive stage		
		Cognitively Unimpaired	**Mild Cognitive Impairment**	**Dementia**
Biomarker Profile	$A^- T^-(N)^-$	normal AD biomarkers, cognitively unimpaired	normal AD biomarkers with MCI	normal AD biomarkers with dementia
	$A^+ T^-(N)^-$	Preclinical Alzheimer's pathologic change	Alzheimer's pathologic change with MCI	Alzheimer's pathologic change with dementia
	$A^+ T^+ (N)^-$ $A^+ T^+(N)^+$	Preclinical Alzheimer's disease	Alzheimer's disease with MCI(Prodromal AD)	Alzheimer's disease with dementia
	$A^+ T^- (N)^+$	Alzheimer's and concomitant suspected non Alzheimer's pathologic change, cognitively unimpaired	Alzheimer's and concomitant suspected non Alzheimer's pathologic change with MCI	Alzheimer's and concomitant suspected non Alzheimer's pathologic change with dementia
	$A^- T^+(N)^-$ $A^- T^-(N)^+$ $A^- T^+(N)^+$	non-Alzheimer's pathologic change, cognitively unimpaired	non-Alzheimer's pathologic change with MCI	non-Alzheimer's pathologic change with dementia

Fig. 1. Biomarker profiles and categories from the NIA-AA research framework. Abbreviations: AD, Alzheimer's disease; MCI, mild cognitive impairment. "Formatting denotes 3 general biomarker 'categories' based on biomarker profiles: those with normal AD biomarkers (no color), those with non-AD pathologic change (dark gray), and those who are in the Alzheimer's continuum (light gray)." Original figure (Table 4) obtained from Jack CR Jr et al. NIA-AA Research Framework: Toward a biological definition of Alzheimer's disease. Alzheimers Dement. 2018; 14(4): 535–562. https://doi.org/10.1016/j.jalz.2018.02.018. PMID: 29653606. Shared under the creative commons license CC BY-NC-ND 4.0.

validated pathophysiological marker for fibrillary amyloid (i.e., neuritic plaques and amyloid angiopathy), which has a strong correlation with a postmortem diagnosis of AD (i.e., approximately 96% concordance), and is, therefore, a good marker for Alzheimer's pathology (Dubois et al., 2014). However, although CSF amyloid biomarkers can indicate a disrupted balance between the production and clearance of Aβ peptide 42 (Aβ$_{1-42}$), PET amyloid can indicate neuritic amyloid plaque accumulation over time (Dubois et al., 2014). CSF Aβ$_{1-42}$ is a measure of Aβ soluble forms, and low concentrations of CSF Aβ$_{1-42}$ suggest significant parenchymal deposition of amyloid (Dubois et al., 2014). In addition to the Aβ burden, tau pathology (i.e., the "T" in the AT(N) classification system) provides a proxy of pathophysiological changes associated with AD. Tau pathology can be assessed through increased levels of CSF p-tau (i.e., hyperphosphorylation of tau in the brain) (Dubois et al., 2014). Neurodegeneration and neuronal injury (i.e., the "N" in the AT(N) classification system) also contribute to the in vivo classification and definition of AD. In this regard, brain glucose metabolism and CSF t-tau are well-established proxies for neurodegeneration; while PET 18F-fluorodeoxyglucose (FDG) uptake is considered a sensitive marker of synaptic dysfunction, accurately mapping regions of hypometabolism associated with clinical symptoms, CSF t-tau is a measure of neuronal damage (Dubois et al., 2014; Jack et al., 2018).

Here, we aim to assess the relation between AT(N) biomarker profiles and brain functional connectivity (FC) because the use of biological definitions at the different stages in the Alzheimer's continuum allows for a better characterization of the disease by considering the biological factors associated with AD, thus permitting to potentially better elucidate the regions or networks associated with cognitive impairment and dementia. The interaction between information shared by different brain regions can be assessed through brain FC measures at rest. FC alludes to the temporal relationship between spatially distant neurophysiological events (Stephan, 2009). Thus, it uses the entire blood-oxygen-level-dependent (BOLD) imaging time series to derive the average connectivity between regions (White, 2019). FC can be assessed at a local and a distant level. Although integrated local correlation analysis is a voxel-to-voxel measure that provides insight into the local function of specific brain regions (Desphande et al., 2009), independent component analysis (i.e., ICA, a voxel-to-voxel data-driven approach) assesses the functional relationship between different brain areas and thus provides insight into between-network connectivity (Wylie et al., 2015). ICA attempts to separate independent sources either

spatially or temporally by organizing brain regions with a similar time course of activation into spatially independent patterns of BOLD signal that are represented as independent components (ICs) (Calhoun, 2001). After separating the brain regions into functional components, the functional coupling of these subcomponents or networks can be assessed, thus creating a proxy for between-network brain connectivity. Together, local correlation and between-network connectivity provide an integrated picture of brain network functioning.

The AT(N) system allows for a biologically based classification, hence a more accurate characterization of the biological events associated with the cognitive impairment in AD and amnestic MCI (aMCI). Consequently, by defining AD and aMCI as biological constructs, rather than by using the clinical definitions, more accurate between-group comparisons can be performed, as these comparisons consider additional confounding factors. Although the AT(N) classification accounts for the biological factors that can confound cognitive deterioration because of Alzheimer's and non-AD pathologic changes, neuropsychiatric syndromes are clinical manifestations that can modulate the expression of cognitive decline in the AD continuum. Neuropsychiatric syndromes associated with AD could provide an understanding of the FC profiles related to the cognitive decline in the AD continuum. Anosognosia is a neuropsychiatric syndrome defined by the unawareness or denial of a neurologic deficit (Langer and Levine, 2014). Anosognosia in patients with mild or moderate AD has a reported incidence proportion between 21.0% and 38.3% and a prevalence between 31.5% and 71.0% (Starkstein et al., 2010; Castrillo-Sanz et al., 2016; Turró-Garriga et al., 2016). Anosognosia for activities of daily living deficits can be present from an early stage of AD with an incidence between 20% and 80% (Starkstein, 2014). The association between brain regions or brain networks and anosognosia is actively pursued as a predictive factor for clinical AD disease progression. Anosognosia of memory deficits has been identified as an independent predictor for the progression of aMCI to AD stage and has been associated with hypometabolism in the posterior cingulate cortex (PCC) and right angular gyrus (Gerretsen et al., 2017). Furthermore, reduced within- and between-network connectivity has been observed in the default mode network (DMN) in AD patients with anosognosia compared with AD patients without anosognosia and cognitively unimpaired participants (Mondragon et al., 2019). Anosognosia has also been associated with disconnection within the medial temporal subsystem of the DMN in AD and aMCI patients (Antione et al., 2019).

This study attempts to address the knowledge gap regarding the brain network FC differences between biologically defined groups within the AD disease continuum, as well as the functional neural substrates of anosognosia in these same groups. The primary objective of this work is to understand the impact of AT(N) biomarker profiles on the local correlation and between-network connectivity among groups of participants with and without Alzheimer's pathologic changes. To achieve this, we assess cognitive decline by comparing groups accounting for the biological profiles at transitional stages of the AD continuum (i.e., aMCI with Alzheimer's pathologic change to AD with Alzheimer's pathologic change and AD with MCI, better known as prodromal AD, compared with AD with dementia) and non-AD cognitive decline (i.e., healthy control [HC] with non-AD pathologic change to aMCI with non-AD pathologic change). Furthermore, we also assess the impact of AD pathologic change on the local correlation and between-network connectivity in aMCI patients (i.e., aMCI with non-AD pathologic change and aMCI with Alzheimer's pathologic change). The secondary objective is to assess the association between anosognosia and regional activation for each of the groups previously described, as well as the impact that anosognosia has on the FC of the regions impacted by anosognosia and the rest of the resting-state brain networks.

2. Methods

Data were obtained from the Alzheimer's Disease Neuroimaging Initiative (ADNI) database (http://adni.loni.usc.edu/data-samples/access-data/). ADNI is a multicenter collaboration launched in 2004, with the common goal of collecting, validating, and using data such as magnetic resonance imaging (MRI) and PET images, genetics, cognitive tests, CSF, and blood biomarkers as biomarkers to define AD progression (Mueller et al., 2005). Participants included in the ADNI project are between the ages of 55 and 90 years, completed at least 6 years of education, and are free of any significant neurologic disease other than AD. With the ultimate goal of developing new treatments and the optimization of clinical trials for aMCI and AD populations, ADNI was initiated in an attempt to define clinical longitudinal changes (e.g., related to clinical diagnosis and neuropsychological assessment) and biomarker (e.g., imaging and CSF) outcome measures (Shaw et al., 2011). ADNI classifies participants into 5 categories: (1) normal aging; (2) subjective cognitive complaints; (3) early MCI; (4) late MCI; and (5) dementia or AD. We searched in the ADNI database for participants with normal aging, early MCI, late MCI, or AD and fMRI sequence available from the ADNI-2 or ADNI Grand Opportunity (ADNI-GO) databases. Perfusion weighted, motion correction, and cerebral blood flow sequences (i.e., which are also classified as fMRI sequences per ADNI definition) were not selected. The entire data set we used was downloaded from the ADNI-2 and ADNI-GO databases beginning on August 28, 2018, and ending on February 15, 2019. Participants with an ADNI-3 advanced sequence were not included in this study for 2 reasons. First, ADNI-2 and the advanced ADNI-3 fMRI versions are not compatible and thus noncomparable; second, at the time of the data extraction for this study, not enough patients had been included in this phase of the ADNI project to merit a separate analysis (more information can be found at http://adni.loni.usc.edu/methods/mri-tool/mri-analysis/). Participant eligibility criteria for ADNI-2 and ADNI-GO are identical and can be found in the ADNI general procedures manual (ADNI-I; http://adni.loni.usc.edu/methods/documents/). The ADNI has developed harmonized standard operating procedures for sample collection, processing, and handling for CSF and serum biomarkers (Shaw et al., 2011). As part of the ADNI, the PET Core initiative focuses on the collection and analysis of metabolic brain imaging. Initially, the ADNI PET Core focused on 18F-FDG PET imaging; however, as ADNI's objectives adjusted to the progressing knowledge in the field of imaging biomarkers, amyloid PET followed by tau PET were introduced into later stages of the ADNI project (Jagust et al., 2015). ADNI was approved by the institutional review boards of all the participating centers. Written informed consent was obtained from all patients. For more information, we refer the reader to www.adni-info.org.

2.1. Description of participants

For our present study, we included 143 participants from the ADNI-2 and ADNI-GO databases who had an rs-fMRI scan and CSF or PET biomarkers available at that time (±4 months) to be used for a later AT(N) classification (Jack et al., 2018). The diagnostic inclusion criteria were based on the ADNI protocols available on the ADNI website. Briefly, clinical diagnosis was assigned to the participants by the site investigators and reassessed at each visit. For this study, we used the diagnosis assigned during the fMRI scan and not the diagnosis the patient had upon enrollment to the ADNI project. Participants with AD diagnosis met the National Institute of Neurologic and Communicative Disorders and Stroke-Alzheimer's Disease and Related Disorders Association criteria for probable AD (McKhann et al., 1984). In addition, mild AD participants had a Mini-Mental State Examination (MMSE) score between 20 and 26 and a global Clinical Dementia Rating (CDR) Scale score of 0.5 or 1.0. MCI is the stage between the expected cognitive decline because of normal aging and the decline because of dementia. Originally, MCI criteria focused on memory impairment or aMCI; however, many subtypes have been described, including nonamnestic (i.e., without memory impairment), as well as single and multidomain impaired forms (Petersen, 2004). aMCI patients had MMSE scores ≥24, a global CDR score of 0.5, objective memory loss as measured by education adjusted scores on the Wechsler Memory Scale Logical Memory II, absence of significant levels of impairment in other cognitive domains, preserved activities of daily living, and absence of dementia. Demographical, neuropsychological, biomarker, and neuroimaging data were extracted from the 2 previously mentioned ADNI data sets (Supplementary Table 1). Exclusion criteria were defined by the ADNI study protocol (Mueller et al., 2005). Functional MRI, fluid-attenuated inverse recovery images, and volumetric T1-weighted images were downloaded for all participants. A Hachinski ischemia score was calculated for every participant at each visit in this study based on the ADNI clinical data regarding dementia clinical characteristics and accompanying signs and symptoms (e.g., onset, evolution, confusion, personality and emotional changes, depression, somatic complaints, history of hypertension and strokes, and focal neurologic signs and symptoms). All patients included had a Hachinski score ≤4. Visual inspection for hyperintensities in the fluid-attenuated inverse recovery sequence to detect possible ischemic lesions was performed by one of the authors (J.D.M.) and corroborated through the "MRI_Infarct" data set to exclude participants with large vascular lesions.

2.2. Cognitive assessment

Cognitive data were extracted from the "ADNIMERGE" file, which incorporates merged data sets containing data from ADNI 1/GO/2 clinical data and numeric summaries. The neuropsychological variables used in the analysis of cognitive changes were the CDR sum of boxes (CDR-SOB), MMSE, Montreal Cognitive Assessment (MoCA), and the 11-item Alzheimer's Disease Assessment Scale-Cognitive Subscale (ADAS-Cog). The global CDR score was calculated from the CDR-SOB, where a CDR-SOB between 0.5 and 4.0 corresponded to a global CDR score of 0.5, a CDR-SOB between 4.5

and 9.0 corresponded to a global CDR score of 1.0, a CDR-SOB between 9.5 and 15.5 corresponded to a global CDR score of 2.0, and a CDR-SOB between 16.0 and 18.0 corresponded to a global CDR score of 3.0 (O'Bryant et al., 2008). Global cognition was assessed through MMSE scores, MoCA scores, and the 11-item ADAS-Cog score.

2.3. In vivo AD biomarker profile: AT(N) classification thresholds

The Aβ burden was evaluated as a continuous and dichotomous variable (i.e., amyloid positive or amyloid negative). The ADNI processes PET imaging data at 4 laboratories that are part of the ADNI PET Core (Jagust et al., 2015). A global cortical threshold for PET amyloid retention to classify patients as PET amyloid positive or PET amyloid negative was used. A participant was classified as PET amyloid positive if the florbetapir (AV-45) PET standardized uptake value ratio (SUVR) was larger than 1.11 based on previous work on the ADNI data (Landau et al., 2013). The global cortical AV-45 PET analyses were segmented and parcellated using freesurfer 4.5.0 (Harvard University, Cambridge MA); all AV-45 PET values were extracted from the ADNI database. As part of the ADNI amyloid PET protocol, the amyloid burden was visually assessed in 6 regions of interest (ROIs; i.e., posterior cingulate, precuneus, parietal, temporal, anterior cingulate, and frontal) to confirm global cortical threshold classification. The second amyloid burden assessment strategy used $A\beta_{1-42}$ CSF levels. The diagnostic threshold for $A\beta_{1-42}$ CSF concentrations to classify participants as positive for amyloid pathology was based on previous work in the ADNI cohort (i.e., $A\beta_{1-42} \leq 192$pg/mL) (Shaw et al., 2009). For this study, patients were classified using PET amyloid.

As ADNI participants did not undergo PET imaging for tau in the ADNI-2 and ADNI-GO study phases, tau burden "T" was assessed by using CSF p-tau levels in this study. The diagnostic thresholds for p-tau$_{181}$ and p-tau$_{181}$/Aβ_{1-42} CSF concentrations to classify participants as having aggregated tau or associated pathologic state were based on previous work in the ADNI cohort (i.e., p-tau$_{181} \geq 23$pg/mL and p-tau$_{181}$/A$\beta_{1-42} \geq 0.1$) (Shaw et al., 2009). Finally, neurodegeneration and neuronal injury "(N)" were assessed using a brain glucose metabolism measure. The previously for the ADNI cohort validated global cortical glucose metabolism mean SUVR threshold of 1.21 (Dowling et al., 2015) was used. This mean SUVR measure is derived from 5 ROIs (i.e., bilateral posterior cingulate gyrus, right and left angular gyri, and middle/inferior temporal gyrus). The AT(N) thresholds previously validated for the ADNI cohort used in this study can be found in Supplementary Table 2.

2.4. Clinical and AT(N) classification

After assessing each biomarker and designating a profile based on the cutoff values previously mentioned, each participant was classified into 3 groups: (1) Alzheimer's pathologic change; (2) non-AD pathologic change; and (3) normal AD biomarkers. Fig. 1 displays the NIA-AA research framework, which divides the 3 AT(N) biomarker types into different biomarker profiles (Jack et al., 2018). For this study, 6 different groups are used: (1) HCs with non-AD pathologic change; (2) aMCI with non-AD pathologic changes; (3) prodromal AD; (4) AD with dementia; (5) aMCI with AD pathology; and (6) clinical AD. For the first 4 groups, we used the NIA-AA research framework definitions; meanwhile, for the fifth group (aMCI with AD pathology), prodromal AD patients and Alzheimer's pathologic change with aMCI are combined. The last group is composed of the clinically classified AD patient group without using the AT(N) classification system. To assess cognitive decline, we defined the groups by the biological factors associated with the AD and non-AD disease continuum according to the AT(N) classification. Furthermore, to assess the impact of Alzheimer's pathologic change (i.e., Alzheimer's pathologic change versus non-AD pathologic change) on FC in clinically defined aMCI patients, between-group comparisons were performed. Four group comparisons were performed; 3 groups assessing the effect of cognitive decline on FC, whereas 1 group comparison assessed the impact of Alzheimer's versus non-AD pathologic change on FC while controlling for cognitive decline: (1) aMCI with Alzheimer's pathologic change versus AD with Alzheimer's pathologic change according to the biological AT(N) profile; (2) prodromal AD versus AD with dementia (i.e., patients with aMCI or AD with biological $A^+T^+(N)^+$ or $A^+T^+(N)-$ profiles); (3) HCs versus aMCI, both with non-AD pathologic change AT(N) profile, to explore the non-AD cognitive decline continuum; and (4) aMCI with non-AD pathologic change AT(N) profile versus aMCI with Alzheimer's pathologic change AT(N) profile: hereby controlling for cognitive decline.

2.5. MRI image acquisition

All MRI scans were performed on Philips 3T MRI scanners, using an eight-channel head matrix coil. High-resolution volumetric T1-weighted images were acquired using a 3D magnetization prepared - rapid gradient echo (MP-RAGE) sequence, with whole-brain coverage and $1 \times 1 \times 1.2$ mm voxel resolution. The rs-fMRI images were acquired using a single-shot T2*-weighted echo-planar sequence collecting 140 volumes, TR of 3000 ms, flip angle of 80°, and 3.3 mm isotropic resolution. The participants kept their eyes open fixed on a point for all rs-fMRI scans. Full descriptions of ADNI MRI image acquisition protocols are available at http://adni.loni.usc.edu/methods/documents/mri-protocols/.

2.5.1. fMRI image preprocessing

The fMRI image preprocessing was performed using the SPM 12 software package (Wellcome Trust Centre for Neuroimaging, University College London, United Kingdom, http://www.fil.ion.ucl.ac.uk/spm/software) implemented in MATLAB (2018b; Mathworks, Natick, MA, USA). All preprocessing steps were performed using the CONN toolbox (Functional Connectivity SPM Toolbox 2017; McGovern Institute for Brain Research, Massachusetts Institute of Technology, http://ww.nitrc.org/projects/conn) following the default preprocessing pipeline for volume-based analyses (Whitfield-Gabrieli and Nieto-Castanon, 2012). The preprocessing included the following steps: (1) realignment and unwarping; (2) slice-timing correction; (3) structural segmentation and normalization; (4) functional normalization; (5) outlier identification; and (6) functional smoothing. After the anatomic and functional preprocessing steps, a denoising step was included to define, explore, and remove possible confounds in the BOLD signal (i.e., unwanted motion, physiological, and other noise sources).

In brief, the first 10 volumes were discarded to allow for equilibration of the magnetic field. All remaining volumes were realigned with the first volume to correct for motion. The realigned images were slice-time corrected, followed by tissue segmentation (i.e., gray matter/white matter/CSF normalized masks were determined) and coregistration to a T1-weighted Montreal Neurological Institute (MNI) native space. Normalization was performed using DARTEL (Ashburner, 2007) with isotropic 2-mm voxels. Outlier identification was performed using Artifact Detection Tools, which computes regressors for outliers and movement (i.e., resulting in scrubbing parameters). Spatial smoothing was performed using an 8 mm full width at half maximum Gaussian kernel. Participant movement realignment and scrubbing parameters (using conservative settings for functional outlier detection settings; global signal z-value threshold and participant motion of 0.5 mm) were assigned as first-level covariates. Quality assurance (QA) plots were visually inspected to detect other possible outliers (i.e.,

"QA_ValidScans," "QA_MaxMotion," and "QA_InvalidScans") and inspected for an adequate match with MNI space and proper coregistration across participants. Preprocessing using the CONN default preprocessing pipeline thus yielded normalized structural volumes, gray matter/white matter/CSF normalized masks, realigned slice-time corrected, and normalized smoothed functional volumes; as well as participant-level movement and scrubbing-related first-level covariates. After the anatomic and functional preprocessing steps, a denoising step was included to define, explore, and remove possible confounds in the BOLD signal. The denoising step applies linear regression and band-pass (i.e., 0.01–0.1 Hz) filtering to remove unwanted motion, white matter, and CSF noise components, as well as physiological noise sources, hence reducing spurious sources of variance in fMRI.

2.5.2. fMRI processing and connectivity analysis

After preprocessing, rs-fMRI data were processed using the CONN toolbox. Local correlation analysis was used as a voxel-to-voxel measure of functional segregation for each observational point. Local correlation is a measure of local functional coupling for each voxel that is determined by the average correlation between the time courses in each seed voxel and its neighbors. A neighborhood of a voxel is defined as the probabilistic region delimited by an isotropic Gaussian kernel. In this study, we used an 8 mm kernel, which is conventionally used by the authors of the CONN toolbox (Whitfield-Gabrieli and Nieto-Castanon, 2012). To determine between-network FC, we used another voxel-to-voxel approach, a group-ICA analysis to identify functional brain networks. The CONN toolbox incorporates an atlas that includes several commonly used functional brain networks (i.e., default mode, sensorimotor, visual, salience, dorsal attention, frontoparietal, language, and cerebellar) and areas (e.g., medial prefrontal cortex, PCC, and left and right lateral parietal cortices). ICA as applied to functional MRI is a data-driven method that attempts to separate independent sources either spatially or temporally by organizing brain regions with a similar time course of activation into spatially independent patterns of BOLD signal that are represented as ICs (Calhoun, 2001). The CONN toolbox follows the general methodology described by Calhoun et al. (2001), which uses a temporal concatenation of BOLD signal data across multiple participants followed by a group-level dimensionality reduction using principal component analysis and fast-ICA for estimation of spatially ICs (Calhoun, 2001). Furthermore, back projection for individual participant-level spatial map estimation is attained by performing dual regression with a univariate spatial-regression step and a multivariate temporal-regression step (Calhoun, 2001). Twenty ICs were chosen as recommended by the CONN toolbox developers, as it allows for adequate characterization and separation of the represented components by matching the IC to a network template via an automated spatial correlation (Whitfield-Gabrieli and Nieto-Castanon, 2012). To this end, a *post hoc* Z-statistic was derived, from the voxel-to-voxel 1-sample *t*-tests of each subject-level ICA spatial map with suprathreshold areas, to help quantify the spatial overlap between ICs and the network template. This statistic, known as the Dice similarity coefficient or Sørensen–Dice index, allowed to assign each IC to a single network. A threshold of 3.5 was selected, as it yielded a one-to-one correspondence between components and networks visualized in the spatial correlation maps (i.e., 1 IC was equal to a single network).

2.6. Anosognosia assessment

Three methods are primarily used to assess anosognosia clinically: (1) measurement instruments that incorporate a discrepancy score between patient and an informant; (2) measurement instruments based on a self-accuracy discrepancy score, in which the patient prospectively attempts to predict their performance on a neuropsychological test; and (3) measurement instruments based on the examiner's judgment. We used the Everyday Cognition scale (ECog) to assess anosognosia. The ECog has been previously used to assess awareness of memory deficits in the ADNI cohort (Gerretsen et al., 2017). The ECog scale evaluates 6 cognitive domains (i.e., memory, language, visuospatial abilities, planning, organization, and divided attention). Each item is evaluated on a 4-point Likert scale that refers to the current condition compared with a period of 10 years or longer ago as follows: 1 = better or no change; 2 = questionable/occasionally worse; 3 = consistently a little worse; and 4 = consistently much worse (Farias et al., 2008). Unawareness of memory deficits (i.e., anosognosia) was determined in the present study using a discrepancy awareness score (i.e., ECog composite score) derived from the difference between the patient's partner report ECog (ECogPR) and the patient's self-reported ECog (ECogSR; i.e., Composite ECog = ECogPR – ECogSR). The raw ECog composite score was then converted to z-scores for each participant, using the mean and standard deviation (SD) from the combined aMCI and AD groups. Higher scores signify greater unawareness of memory deficits by the patient and hence anosognosia. We decided to use the ECog composite z-score, rather than establishing cutoff values (i.e., ±1.5 SD) to explore the effect of unawareness of memory deficits (i.e., anosognosia) on the FC of each group in this study (i.e., a general linear model [GLM] that includes anosognosia as a regressor and thus assesses the individual effect of awareness of memory deficits in each group of interest).

2.7. Statistical analysis

Statistical analysis was performed using SPSS 25 (SPSS Inc., Chicago, IL, USA). Data were screened for outliers and tested for normality assumptions. The normality of continuous variables was assessed with the Shapiro-Wilk normality test and visually using histograms and Q-Q plots. For variables with nonnormal distribution, a Wilcoxon rank-sum test was used. Analysis of variance (ANOVA) was used for subgroup-level analysis for normally distributed variables, and a Kruskal-Wallis test was used for nonparametric variables. Fisher's exact test was used to evaluate the association between discrete variables and groups. For voxel-level measurements, two-sample paired *t*-tests were performed on mean regional activation maps to assess between-group differences for the group-ICA and the local correlation analysis; the statistical significance was set at $p \leq 0.05$ false discovery rate (FDR)-corrected for cluster size. To correct for unbalanced group comparisons, we performed conjunction analyses using different contrasts [–1 1 0] and [–1 –1 2]. This conjunction analysis allows to correct for a low power/sensibility bias by looking into the remnant effect size of the between-group differences (Friston et al., 1999). In group-level ANOVA designs, conjunction analysis allows for the comparison between 2 groups (FC_{ab}) by excluding the observed difference to a third group ($FC_{ac} - FC_{bc}$), with the connections present in both contrasts corrected for a low power/sensitivity bias). The connectivity maps (i.e., regional activation maps or beta maps) were used to assess the correlation between anosognosia and brain activation. A voxel-wise linear regression analysis was performed to assess the simple main effect of anosognosia on the mean regional activation; the statistical significance was set at $p \leq 0.05$ FDR-corrected for cluster size. Using the first-level ICA, a second-level FC analysis was performed through voxel-to-voxel simple *t*-tests between the regions with high variance explained by anosognosia and the identified ICA networks. The statistical significance for the FC analysis was also set at $p \leq 0.05$ FDR-corrected for cluster size. To

further assess the strength of the association between anosognosia and the connectivity maps, a correlation analysis between anosognosia and the FC variance within each IC (i.e., a voxel-wise regression analysis between the ECog composite z-score and the intrinsic connectivity residuals) was performed. An ROI FC analysis was performed between the regions that were highly correlated to anosognosia and the 8 major brain resting-state networks. Finally, to assess the effect of other covariates that could contribute to FC between-group differences, first, an overall voxel-wise regression analysis was performed using a 6×121 second-level covariate matrix followed by voxel-wise regression analyses with backward elimination of the following variables: age, sex, ethnicity, APOE status, Hachinski ischemia score, and education.

3. Results

3.1. Participant characteristics

One hundred and forty-three participants had a structural and an rs-fMRI scan (i.e., same visit), as well as CSF or PET biomarkers available from the same time point (±4 months). The full description of demographic, diagnostic, and cognitive participant characteristics can be found in Table 1, whereas cognitive characteristics are displayed by clinical diagnosis in Fig. 2. Twelve participants (i.e., 5 HC and 7 aMCI) had missing information regarding1 biomarker, which did not permit an accurate AT(N) classification. Ten participants were removed (i.e., 2 HC, 7 aMCI, and 1 AD) from the rs-fMRI analysis because of excessive head movement, leaving 121 participants in total (i.e., 26 HC, 78 aMCI, and 17 AD). Fig. 3 displays a stepwise analysis of the patient selection and grouping by their biomarker profile.

3.2. AT(N) biomarker profile

The participants included in this study were classified according to the 2018 NIA-AA research framework, and the biomarker profiles are displayed in Fig. 1 (Jack et al., 2018). Overall, 67 participants had a biomarker profile compatible with Alzheimer's pathologic change (i.e., 6 HC, 44 aMCI, and 17 AD), 47 had a non-AD pathologic change profile (i.e., 20 HC and 27 aMCI), and 7 had a normal biomarker profile (i.e., 7 aMCI). According to the descriptive nomenclature described by Jack Jr. and collaborators (2018), the HC participant group had 3 participants with preclinical AD, 3 with Alzheimer's and concomitant suspected non-Alzheimer's pathologic change, cognitively unimpaired, and 20 with non-Alzheimer's pathologic change, cognitively unimpaired. Among the aMCI patients, 32 patients had AD with aMCI (i.e., prodromal AD; 23 $A^+T^+(N)^+$ and 9 $A^+T^+(N)-$), 7 participants had Alzheimer's and concomitant suspected non-Alzheimer's pathologic change with aMCI, 5 participants had Alzheimer's pathologic change with aMCI, 27 participants had non-Alzheimer's pathologic change with aMCI, and 7 participants had aMCI with a normal biomarker profile. Among the patients clinically diagnosed with AD, all had an AT(N) profile compatible with Alzheimer's pathologic change. Specifically, 14 patients had AD with dementia (i.e., 3 $A^+T^+(N)^+$ and 11 $A^+T^+(N)-$), 1 patient had Alzheimer's and concomitant suspected non-Alzheimer's pathologic change with dementia, and 2 patients had Alzheimer's pathologic change with dementia. For a detailed breakdown of the AT(N) biomarker profile classification by clinical diagnostic group and into Alzheimer's pathologic change, non-AD pathologic change, and normal biomarker grouping, we refer the reader to Table 2. Three group comparisons assessing the effect of cognitive decline on FC were performed: (1) aMCI with Alzheimer's pathologic change according to the biological AT(N) profile (n = 44 participants) versus AD with Alzheimer's pathologic change (n = 17); (2) prodromal AD

Table 1
Demographics and cognitive participant characteristics

Diagnosis	N	Demographical						Cognition			
		Sex	Age	Ethnicity	Marital status	APOE ε4 status	Education	CDR sum of boxes	MMSE	MoCA	ADAS-Cog
Overall	143	79 female (55.2%)	72.97 ± 7.62 (range, 56–95)	128 White 5 Hispanic 4 African American 3 Mixed 3 Asian	107 Married 15 Divorced 15 Widowed 6 Never married	74 Negative 49 Positive 18 Other 2 Missing	16.20 ± 2.67 (8–20)	1.63 ± 1.61 (0–7.0)	27.45 ± 2.58 (19–30)	23.23 ± 3.87 (6–29)	10.21 ± 6.45 (1–37)
HC	33	20 Female (60.6%)	74.70 ± 7.24 (65–95)	26 White 3 Hispanic 3 African American 1 Mixed	25 Married 3 Divorced 2 Widowed 3 Never married	21 Negative 10 Positive 1 Other 1 Missing	16.82 ± 2.11 (12–20)	0.05 ± 0.71 (0–3.0)	28.76 ± 1.37 (25–30)	25.21 ± 2.19 (21–29)	5.71 ± 2.91 (2–14)
aMCI	92	48 Female (52.2%)	72.28 ± 7.62 (56–89)	85 White 2 Hispanic 1 African American 2 Mixed 2 Asian	67 Married 11 Divorced 11 Widowed 3 Never married	51 Negative 29 Positive 11 Other 1 Missing	16.22 ± 2.80 (8–20)	1.66 ± 1.13 (0–6.5)	27.92 ± 1.81 (23–30)	23.53 ± 3.11 (14–29)	9.51 ± 4.31 (1–22)
AD	18	11 Female (61.1%)	73.33 ± 8.14 (56–87)	17 White 1 Asian	15 Married 1 Divorced 2 Widowed	2 Negative 10 Positive 6 Other	14.94 ± 2.56 (12–20)	4.36 ± 1.37 (2.0–7.0)	22.61 ± 2.23 (19–26)	17.76 ± 5.19 (6–25)	22.00 ± 6.52 (10–37)

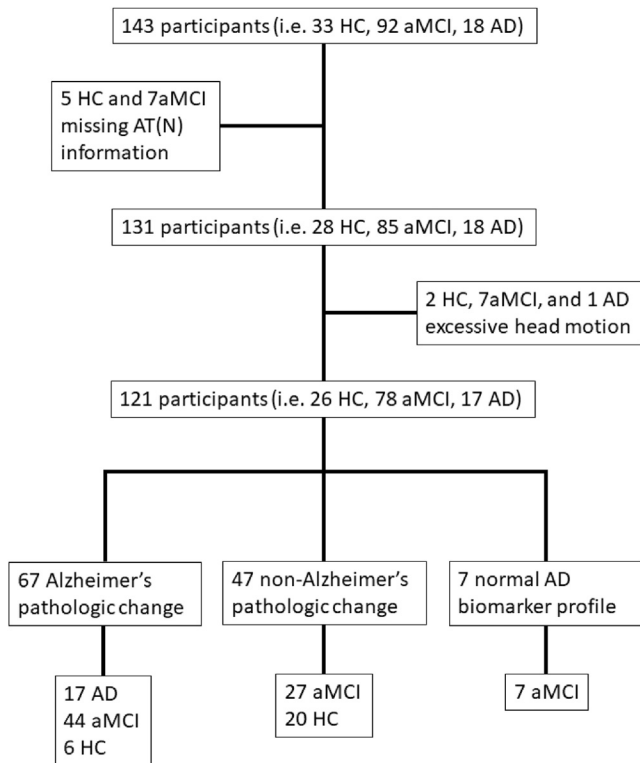Mean ± standard deviation where applicable.
Key: AD, Alzheimer's disease; ADAS-Cog, 11-item Alzheimer's Disease Assessment Scale-Cognitive Subscale; aMCI, amnestic mild cognitive impairment; APOEε4, apolipoprotein E ε4 genotyping; CDR, Clinical Dementia Rating; HC, cognitively normal healthy controls; MMSE, Mini-Mental Sate Examination; MoCA, Montreal Cognitive Assessment.
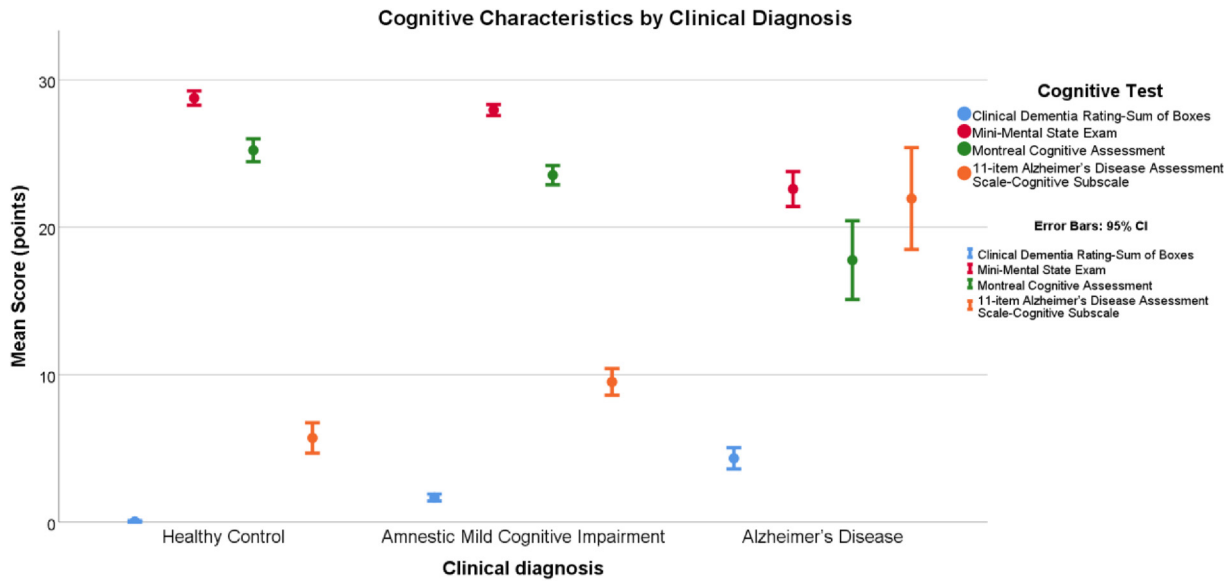
Fig. 2. Cognitive characteristics by clinical diagnosis. Graphical representation of the cognitive characteristics displayed by the clinical diagnosis groups. Presented are the group means and the 95% confidence interval of the 4 cognitive assessment instruments: the Clinical Dementia Rating Scale- Sum of Boxes; the Mini-Mental State Examination; the Montreal Cognitive Assessment; and the 11-item Alzheimer's Disease Assessment Scale-Cognitive Subscale.

or AD with aMCI (i.e., aMCI with $A^+T^+(N)^+$ and $A^+T^+(N)-$, n = 32) versus AD with dementia (i.e., AD with $A^+T^+(N)^+$ and $A^+T^+(N)-$, n = 14); and (3) HCs (n = 20) versus aMCI (n = 27), both with non-AD pathologic change AT(N) profile. Meanwhile, 1 group comparison was also performed that assessed the impact of the biological profile on FC, while controlling for cognitive decline, among aMCI patients

Fig. 3. Patient selection and grouping by biomarker profile. Abbreviations: HC, healthy control; aMCI, amnestic mild cognitive impairment; AD, Alzheimer's disease clinical diagnosis; AT(N), research framework biological classification based on in vivo biomarkers.

(i.e., 4) aMCI with non-AD pathologic change AT(N) profile (n = 27) versus aMCI with Alzheimer's pathologic change AT(N) profile (n = 44). For a graphical representation of the between-group comparisons, we refer the reader to the graphical abstract. Sex, age, ethnicity, marital status, APOEε4 status, education, MMSE, MoCA, and ADAS-Cog were assessed for between-group statistical differences, and none were found.

3.3. FC analysis of cognitive decline

First, a local correlation analysis was performed to determine the regional functional coupling to assess the activity of specific brain regions without a priori knowledge of functional and structural brain communication (Deshpande et al., 2009). A neighborhood was determined to explore the correlation between adjacent voxels, which provided insight into the cohesiveness or functional segregation of each region. Second, ICA were performed to assess the relationship between different brain areas. As a voxel-to-voxel measure of brain functional integration, ICA allows the assessment of the functional coupling of distant networks (Wylie et al., 2015). Twenty ICs were chosen, as recommended by the CONN toolbox developers, as it allows for adequate characterization and separation of the represented components by matching the IC to a network template via an automated spatial correlation (see Supplementary Fig. 1 that displays the spatial correlation of ICs to the template). A large spatial correlation corresponds to a better match to the network template. After matching, the following components were identified: components 1, 5, 10, 13, and 17 best corresponded to the cerebellar network; components 2, 3, 11, and 12 (i.e., right temporal pole) to the DMN; components 4 and 14 to the dorsal attention networks; components 6, 15, 18, and 19 (i.e., thalamus) to the sensorimotor network; components 7, 8, and 16 to the visual network; component 9 to the language network; and component 20 to CSF. Brain network dynamics of cognitive decline through different stages of the cognitive decline continuum were assessed by considering the biological definitions based on the AT(N) classification. We present the results of the between-group comparisons that assess the differences in FC between patients with (1) clinical AD (i.e., all with Alzheimer's pathologic change)

Table 2
AT(N) biomarker profile classification by clinical diagnostic group

AT(N) biomarker profile												
	Alzheimer's pathologic change					Non-AD pathologic change				Normal AD biomarkers		
Group	A+ T+ (N)+	A+ T+ (N)−	A+ T− (N)+	A+ T− (N)−	Total	A− T+ (N)+	A− T+ (N)−	A− T− (N)+	Total	A− T− (N)−		Total
AD	3	11	1	2	17	0	0	0	0	0		17
aMCI	23	9	7	5	44	8	1	18	27	7		78
HC	3	0	3	0	6	8	0	12	20	0		26
Total	29	20	11	7	67	16	1	30	47	7		121

AT(N): National Institute on Aging-Alzheimer's Association (NIA-AA) 2018 research framework for a biological in vivo classification based on "A" beta-amyloid burden, "T" tau pathology, and "N" neurodegeneration or neuronal injury.
Key: AD, Alzheimer's disease; aMCI, amnestic mild cognitive impairment; HC, cognitively normal healthy controls.

and aMCI with Alzheimer's pathologic change; (2) prodromal AD (i.e., AD with aMCI) and AD with dementia; and (3) cognitively unimpaired (i.e., HCs with non-AD pathologic change) and aMCI patients with non-AD pathologic change. For the last comparison, the effect of biological disease burden on FC in aMCI is explored (i.e., 4) by comparing aMCI patients with Alzheimer's pathologic change to aMCI patients with non-AD pathologic change, thereby controlling for cognitive decline.

3.3.1. aMCI with Alzheimer's pathologic change versus AD with Alzheimer's pathologic change patients

a) Local correlation analysis

Patients with aMCI and Alzheimer's pathologic changes had greater local correlation than AD with Alzheimer's pathologic change patients in the DMN (T = 6.86, p-FDR < 0.001) and the salience network (T = 8.23; p-FDR < 0.001). Conversely, AD with Alzheimer's pathologic change patients had higher local correlation than aMCI patients with Alzheimer's pathologic change in the cerebellar network (T = 9.21, p-FDR < 0.001) and the sensorimotor network (T = 3.21, p-FDR = 0.002). These results as well as the cluster size and localization (i.e., region and peak activation MNI coordinates) are presented in the right column of Table 3 and visually represented on the left side of Fig. 4A.

b) Group-ICA analysis

Patients with aMCI and AD pathologic changes had greater between-network connectivity than AD with Alzheimer's pathologic change patients between the cerebellar network and DMN (T = 3.33; p-FDR = 0.003) and between the dorsal attention and salience networks (T = 2.94; p-FDR = 0.0094). Conversely, AD with Alzheimer's pathologic change patients had greater between-network connectivity than aMCI patients with Alzheimer's pathologic change between the cerebellar and visual networks (T = 3.01; p-FDR = 0.0076). Cluster location, size, and activation effect sizes are displayed in the left column of Table 3 and visually represented on the right side of Fig. 4A.

3.3.2. Prodromal AD (AD with aMCI) versus AD with dementia

a) Local correlation analysis

Patients with prodromal AD had greater local correlation than AD with dementia patients in the DMN (T = 8.26; p-FDR < 0.001; T = 6.70, p-FDR < 0.001; T = 6.67; p-FDR < 0.001; here, each T-value represents a separate cluster within a particular network). Conversely, AD with dementia patients had greater local correlation than patients with prodromal AD in the cerebellar network (T = 6.88; p-FDR < 0.001) and

the sensorimotor network (T = 6.73; p-FDR < 0.001). Cluster location, size, and activation effect sizes are found in the right column of Table 4 and visually represented on the left side of Fig. 4B.

b) Group-ICA analysis

The prodromal AD group had greater between-network connectivity than AD patients with dementia between the DMN and the cerebellar network (T = 4.01; p-FDR < 0.001), as well as between the DMN and the sensorimotor network (T = 2.39; p-FDR = 0.0351) and between the cerebellar and visual networks (T = 4.01; p-FDR = 0.0012). Conversely, the between-network connectivity was greater in AD patients with dementia than in prodromal AD between the DMN and the sensorimotor network (T = 3.03; p-FDR = 0.0203; T = 2.83, p-FDR = 0.0352; T = 2.21, p-FDR = 0.041; here, each T-value represents a separate cluster within a particular network), between the DMN and the dorsal attention network (T = 2.81, p-FDR = 0.0185), between the DMN and the cerebellar network (T = 2.80; p-FDR = 0.0375; T = 2.50, p-FDR = 0.0402), between the DMN and the visual network (T = 2.61; p-FDR = 0.0308), and between the visual and sensorimotor networks (T = 2.80, p-FDR = 0.0308). Cluster location, size, and activation effect sizes are found in the left column of Table 4 and visually represented on the right side of Fig. 4B.

3.3.3. HCs versus aMCI both with non-AD pathologic change

a) Local correlation analysis

Patients with aMCI with non-AD pathologic change had greater local correlation than cognitively healthy participants with non-AD pathologic change in the cerebellar network (T = 7.92; p-FDR < 0.001), the visual network (T = 7.92, p-FDR < 0.001), and the sensorimotor network (T = 6.65; p-FDR < 0.001). There were no significant results for the reverse comparison. Cluster location, size, and activation effect sizes are found in the right column of Table 5 and visually represented on the left side of Fig. 4C.

b) Group-ICA analysis

The between-network connectivity was greater in aMCI patients with non-AD pathologic change than in participants with normal cognition and non-AD pathologic change between the visual and sensorimotor networks (T = 2.94; p-FDR = 0.0052; T = 2.89, p-FDR = 0.0058; here, each T-value represents a separate cluster within a particular network) and between the visual and cerebellar networks (T = 2.64, p-FDR = 0.011). There were no significant results for the reverse comparison. Cluster location, size, and activation effect sizes are found in the left column of Table 5 and visually represented on the right side of Fig. 4C.
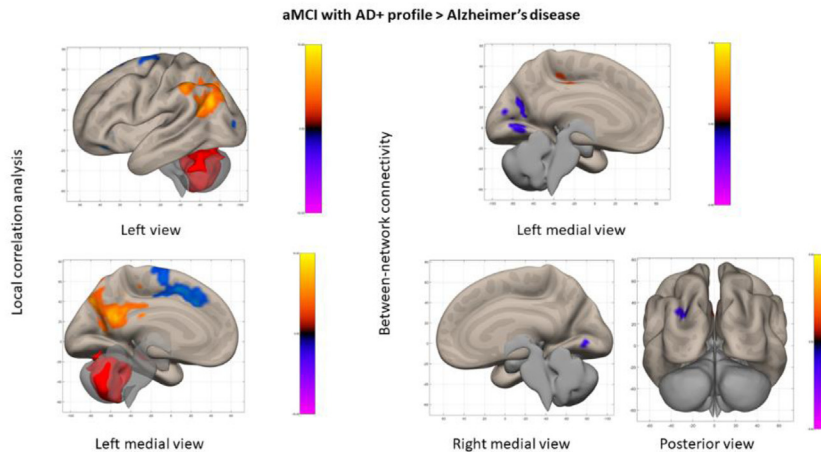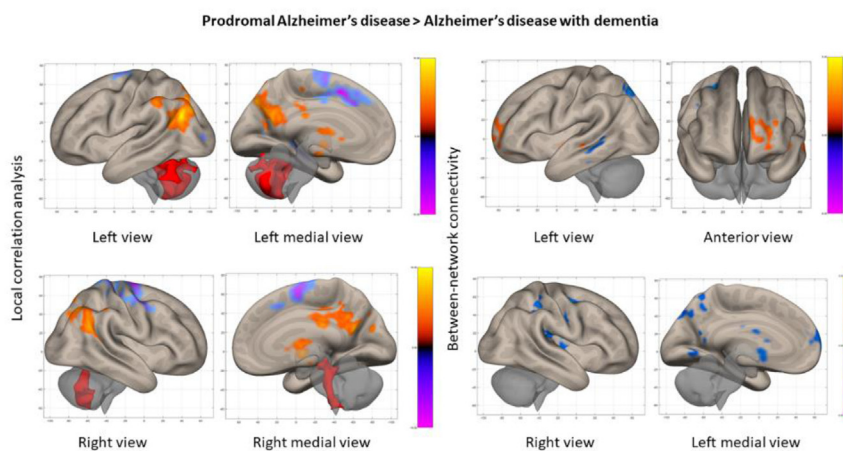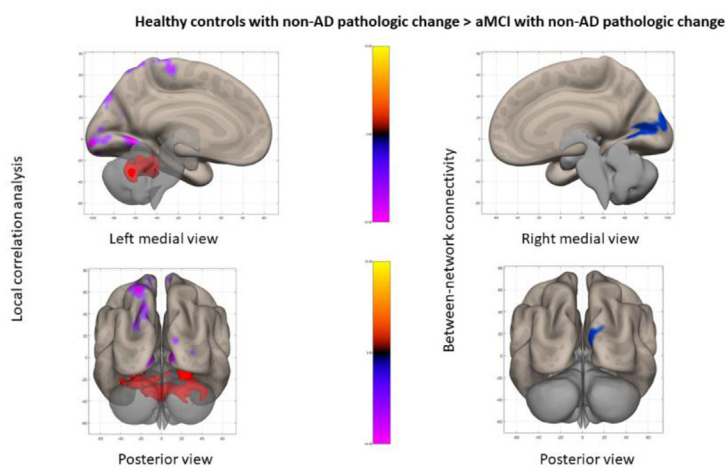
Table 3
Functional connectivity analysis between aMCI with Alzheimer's pathologic change and AD with Alzheimer's with pathologic change patients

aMCI with Alzheimer's pathologic change > AD with Alzheimer's with pathologic change							
Local correlation analysis				**Between-network connectivity**			
Networks[a]	Region (peak activation coordinate)	Cluster size (voxels)	Effect size[b] (p-FDR)	Networks[a]	Region (peak activation coordinate)	Cluster size (voxels)	Effect size[b] (p-FDR)
Default mode	Left lateral occipital cortex (−56 −72 +22)	1810	T = 6.86 (<0.001)	Cerebellar and default mode	Precuneus (−17 −68 +26)	29	T = 3.33 (0.003)
	Bilateral precuneus cortex (−07 −71 +38) (+04 −48 +37)	1143 945		Dorsal attention and salience	Left precentral gyrus (−13 −33 +45)	32	T = 2.94 (0.0094)
	Left posterior cingulate cortex (−07 −55 +25)	365					
	Left angular gyrus (−50 −64 +23)	282					
	Left supramarginal gyrus (−56 −46 +45)						
Salience	Right lateral occipital cortex (+56 −60 +33)	884	T = 8.23 (<0.001)	Cerebellar and visual	Left lateral occipital cortex (−30 −72 +27)	127	T = −3.01 (0.0076)
	Right angular gyrus (+45 −46 +24)	681			Left lingual gyrus (−07 −71 +01)	89	
	Right insular cortex (+39 −16 −02)	175			Left intracalcarine cortex (−12 −79 +14)	66	
	Right supramarginal gyrus (+45 −61 +50)	157			Left cuneal cortex (−03 −82 +16)	33	
	Right putamen (+28 −14 +10)	89			Right lingual gurus (+07 −74 +01)	33	
Cerebellar	Left cerebellum VIII (−08 −68 −38)	1054	T = −9.21 (<0.001)		Right supracalcarine cortex (+03 −81 +05)	26	
	Left cerebellum crus 1 (−27 −66 −33)	1022					
	Right cerebellum VIII (+13 −66 −54)	738					
	Left cerebellum VI (−28 −66 −32)	685					
	Right cerebellum crus 1 (+38 −64 −33)	604					
	Left cerebellum crus 2 (−29 −64 −33)	556					
	Right cerebellum VI (+33 −70 −30)	453					
Sensorimotor	Right superior frontal gyrus (+18 −07 +58)	460	T = −3.21 (0.002)				
	Right precentral gyrus (+11 −04 +56)	363					
	Right juxtapositional lobule (+38 −07 +49)	277					
	Left superior frontal gyrus (−08 +23 +45)	254					

Key: AD, Alzheimer's disease; aMCI, amnestic mild cognitive impairment.
[a] Characterization of each network is derived from the spatial overlap between the CONN network template and the local correlation between-group differences or the independent component (IC) between-group differences.
[b] Effect size refers to the statistical inference derived from the T-value or the size of the difference relative to the variation of the data (i.e., differences in the mean regional activation between groups for a specific region or cluster, for the local correlation analysis, and an independent component for the IC analysis). Multiple t-values correspond to more than 1 independent cluster within the same network with a high local correlation difference between the compared groups or to multiple regions (i.e., clusters) inside an independent component.

A   **Assessing the impact of cognitive decline in symptomatic Alzheimer's pathologic change**

aMCI with AD+ profile > Alzheimer's disease

B   **Assessing the impact of cognitive decline in Alzheimer's disease continuum**

Prodromal Alzheimer's disease > Alzheimer's disease with dementia

C   **Assessing the impact of early symptomatic non-AD pathologic change**

Healthy controls with non-AD pathologic change > aMCI with non-AD pathologic change

Fig. 4. Functional connectivity analysis of cognitive decline. (A) Functional connectivity analysis between aMCI with Alzheimer's pathologic change and AD with Alzheimer's with pathologic change patients. FC, functional connectivity; aMCI, amnestic mild cognitive impairment; AD, Alzheimer's disease. Activation maps are graphical representations of Table 3, where hot colors represent greater mean regional activation (i.e., between clusters for the local correlation analysis and between specific region and independent component for the between-network functional connectivity analysis) in aMCI with Alzheimer's pathologic change than AD with Alzheimer's with pathologic change patients and cold colors represent the opposite contrast or lower mean regional activation (i.e., cold colors reflect the opposite effect, greater mean regional activation in AD with Alzheimer's with pathologic change patients than in aMCI with Alzheimer's pathologic change). Subcortical activation is represented in red. Activation values based on T values (i.e., activation color bar range −10 to 10 for the local correlation analysis and −5 to 5 for the between-network connectivity analysis). ICA figures display the cluster within the independent component where the between-group differences are observed and not the connectivity between regions; the color gradients are proportional to the size of the effect (i.e., between-

3.3.4. aMCI with non-AD pathologic change versus aMCI with Alzheimer's pathologic change

a) Local correlation analysis

Patients with aMCI with Alzheimer's pathologic change had greater local correlation than aMCI patients with non-AD pathologic change in the cerebellar network (T = 6.41, p-FDR = 0.001) and the visual network (T = 6.32; p-FDR < 0.001). There were no significant results for the reverse comparison. Cluster location, size, and activation effect sizes are found in the right column of Table 6 and visually represented on the left side of Fig. 5.

b) Group-ICA analysis

Greater between-network connectivity was observed in aMCI patients with non-AD pathologic change than in aMCI patients with Alzheimer's pathologic change between the dorsal attention and cerebellar networks (T = 3.96; p-FDR < 0.001), between the visual and cerebellar networks (T = 3.29; p-FDR = 0.0016), between the default mode and cerebellar networks (T = 2.58; p-FDR = 0.0241), and between the visual and dorsal attention networks (T = 2.34; p-FDR = 0.0438). Conversely, aMCI patients with Alzheimer's pathologic change had greater between-network connectivity between the salience and visual networks (T = 2.58; p-FDR = 0.0238) than patients with aMCI with non-AD pathologic change. Cluster location, size, and activation effect sizes are found in the left column of Table 6 and visually represented on the right side of Fig. 5.

3.4. Neural correlates of anosognosia

A voxel-vise regression analysis was performed on each clinically and biologically defined group with cognitive decline to understand the neural correlates of anosognosia in the Alzheimer's continuum. From the sample included in this study, several participants lacked a complete set of ECog scores to obtain an ECog composite z-score. Seventy-eight AD or aMCI patients had AT(N) biomarkers and fMRI data, of which 73 also had complete ECog data for that same visit (i.e., 37 aMCI with Alzheimer's pathologic change, 19 aMCI with non-AD pathologic change, and 17 AD patients). Furthermore, among the subgroups analyzed, 32 patients with prodromal AD and 14 patients with AD with dementia had the ECog data necessary to calculate the ECog composite z-score.

We explored the impact of anosognosia among each group previously described. After the regression analyses assessing the relation between anosognosia and brain FC, we found that only the prodromal AD group had an association (i.e., positive) between anosognosia and brain connectivity in the bilateral anterior cingulate cortex (ACC; T = 2.52, p-FDR = 0.043); in other words, the greater the anosognosia, the stronger the FC. This however only

provided information on the ACC being correlated to anosognosia in prodromal AD. A second-level FC analysis was used to further explore the observed between-network connectivity between the ACC and the 8 major resting-state brain networks in prodromal AD. In this analysis, a seed to voxel analysis using the ACC as the ROI or seed was used to assess its FC with the 8 resting-state brain networks. This allowed us to understand the relation between anosognosia and the FC between the ACC and the rest of the brain in prodromal AD. Among patients with anosognosia in prodromal AD, the FC between the ACC and the visual (T = 3.72; p-FDR ≤ 0.001), the language (T = 3.25; p-FDR = 0.0029), and the sensorimotor (T = 2.40; p-FDR = 0.0233) networks was increased. Conversely, in this group, FC between the ACC and the DMN (T = −3.34; p-FDR = 0.0023) and cerebellar (T = −3.20; p-FDR = 0.0033) networks was decreased. Cluster location, size, and effect sizes are found in Table 7 and visually represented in Fig. 6. To further illustrate the identified relationship between anosognosia and the FC between the ACC and the other resting-state networks, we provide the scatterplots correlating the intrinsic connectivity residuals and the ECog composite Z-score in Supplementary Fig. 2 and the effect sizes of this relationship in Supplementary Table 3. Finally, no significant effects were observed in the second-level covariate voxel-wise regression analysis with backward elimination of age, sex, ethnicity, APOE status, Hachinski ischemia score, and education.

4. Discussion

To the best of our knowledge, this is the first study that incorporates the NIA-AA research framework to assess differences in FC between different stages in the AD continuum. Furthermore, we also identified neural correlates of anosognosia in clinically and biologically characterized groups in the AD continuum. We report that using biological definitions, the DMN connectivity is persistently affected in the early stages of the Alzheimer's biological continuum, which is on par with findings from clinically defined groups in the AD continuum. Furthermore, we associate anosognosia to FC changes in the ACC in prodromal AD and between the ACC and different brain networks, pointing to the importance of the ACC in the perception of awareness of memory deficits and how brain FC changes in this region might precede changes found in the PCC, a DMN region typically associated in AD with anosognosia.

Cognitive decline was assessed objectively by considering biological confounding factors, which can be identified through the AT(N) characterization. In this study, we measured the local correlation and between-network connectivity changes throughout the Alzheimer's syndromal and biological disease continuum. First, we considered biological confounding factors associated with AD by making group comparisons that consider Alzheimer's pathologic change (i.e., $A^+T^-(N)^-$, $A^+T^-(N)^+$, $A^+T^+(N)^-$, and $A^+T^+(N)^+$ biological profiles). In addition, Alzheimer's pathologic change was

group differences t-values). (B) Functional connectivity analysis between prodromal AD and AD with dementia. FC, functional connectivity; AD, Alzheimer's disease. Activation maps are graphical representations of Table 4, where hot colors represent greater mean regional activation (i.e., between clusters for the local correlation analysis and between specific region and independent component for the between-network functional connectivity analysis) in prodromal AD than AD patients with dementia and cold colors represent the opposite contrast or lower mean regional activation (i.e., cold colors reflect the opposite effect, greater mean regional activation in AD patients with dementia than in prodromal AD). Subcortical activation is represented in red. Activation values based on T values (i.e., activation color bar range −10 to 10 for the local correlation analysis and −5 to 5 for the between-network connectivity analysis). ICA figures display the cluster within the independent component where the between-group differences are observed and not the connectivity between regions; the color gradients are proportional to the size of the effect (i.e., between-group differences t-values). (C) Functional connectivity analysis between HC with non-AD change and aMCI with nonpathologic change. Abbreviations: FC, functional connectivity; HC, cognitively healthy participants; AD, Alzheimer's disease; aMCI, amnestic mild cognitive impairment. Activation maps are graphical representations of Table 5, where hot colors represent greater mean regional activation (i.e., between clusters for the local correlation analysis and between specific region and independent component for the between-network functional connectivity analysis) in HC with non-AD pathologic change than aMCI patients with non-AD pathologic change, and cold colors represent lower activation group differences (i.e., cold colors reflect the opposite effect, greater mean regional activation in aMCI patients with non-AD pathologic change than in HC with non-AD pathologic change). Subcortical activation is represented in red. Activation values based on T values (i.e., activation color bar range −10 to 10 for the local correlation analysis and −5 to 5 for the between-network connectivity analysis). ICA figures display the cluster within the independent component where the between-group differences are observed and not the connectivity between regions; the color gradients are proportional to the size of the effect (i.e., between-group differences t-values). (For interpretation of the references to color in this figure legend, the reader is referred to the Web version of this article.)

Table 4

Functional connectivity analysis between prodromal AD and AD with dementia

Prodromal AD > Alzheimer's disease with dementia

Local correlation analysis				Between-network connectivity			
Networks[a]	Region (peak activation coordinate)	Cluster size (voxels)	Effect size[b] (p-FDR)	Networks[a]	Region (peak activation coordinate)	Cluster size (voxels)	Effect size[b] (p-FDR)
Default mode	Right lateral occipital cortex ($+44$ -60 $+52$)	1179	T = 8.26 (<0.001)	Cerebellar and default mode	Left frontal pole (-32 $+50$ $+18$)	493	T = 4.01 (0.0012)
	Right angular gyrus ($+54$ -60 $+32$)	654	T = 6.70 (<0.001)	Sensorimotor and default mode	Left planum polare (-43 -13 -07)	49	T= 2.39 (0.0351)
	Right supramarginal gyrus ($+54$ -47 $+50$)	122	T = 6.67 (<0.001)	Sensorimotor and default mode	Right parietal operculum cortex ($+46$ -30 $+19$)	89	T = -3.03 (0.0203)
	Brain stem ($+08$ -30 -14)	790			Right planum temporale ($+42$ -20 $+04$)	33	T = -2.83 (0.0352)
	Left lateral occipital cortex (-54 -74 $+22$)	1724			Left paracingulate gyrus (-07 $+51$ $+09$)	38	T = -2.21 (0.041)
	Left precuneus cortex (-09 -72 $+40$)	995		Dorsal attention and default mode	Left middle temporal gyrus (-48 -26 -20)	159	T = -2.81 (0.0185)
	Posterior cingulate cortex (-05 -58 $+23$)	607					
	Left angular gyrus (-42 -66 $+24$)	350					
	Left supramarginal gyrus (-58 -44 $+42$)	195					
Cerebellar	Left cerebellum VIII (-16 -62 -52)	856	T = -6.88 (<0.001)	Default mode and cerebellar	Left inferior temporal gyrus (-48 -26 -20)	37	T = -2.80 (0.0375)
	Left cerebellum Crus 1 (-48 -65 -38)	767			Posterior cingulate cortex ($+12$ -41 $+30$)	91	T = -2.50 (0.0402)
	Right cerebellum VIII ($+14$ -68 -52)	623		Default mode and visual	Left precuneus (-18 -70 $+46$)	545	T = -2.61 (0.0308)
	Left cerebellum VI (-44 -61 -25)	534			Left lateral occipital cortex (-20 -72 $+45$)	142	
	Left cerebellum Crus 2 (-48 -65 -37)	235					
Sensorimotor	Right precentral gyrus ($+14$ -14 $+70$)	907	T = -6.73 (<0.001)	Visual and sensorimotor	Right precentral gyrus ($+26$ -04 $+46$)	62	T = -2.80 (0.0308)
	Right postcentral gyrus ($+12$ -15 $+67$)	449					
	Right juxta-positional lobule ($+42$ -07 $+50$)	386					
	Left juxta-positional lobule (-19 -11 $+70$)	283					
	Left superior frontal gyrus (-10 $+21$ $+39$)	269					
	Right superior frontal gyrus ($+45$ $+07$ $+42$)	268					
	Left paracingulate gyrus (-08 $+10$ $+48$)	260					

Key: AD, Alzheimer's disease; aMCI, amnestic mild cognitive impairment.

[a] Characterization of each network is derived from the spatial overlap between the CONN network template and the local correlation between-group differences or the independent component (IC) between-group differences.

[b] Effect size refers to the statistical inference derived from the T-value or the size of the difference relative to the variation of the data (i.e., differences in the mean regional activation between groups for a specific region or cluster, for the local correlation analysis, and an independent component for the IC analysis). Multiple t-values correspond to more than 1 independent cluster within the same network with a high local correlation difference between the compared groups or to multiple regions (i.e., clusters) inside an independent component.

Table 5
Functional connectivity analysis between HC and aMCI with non-AD change

HC with non-AD pathologic change > aMCI with non-AD pathologic change

Local correlation analysis				Between-network connectivity			
Networks[a]	Region (peak activation coordinate)	Cluster size (voxels)	Effect size[b] (p-FDR)	Networks[a]	Region (peak activation coordinate)	Cluster size (voxels)	Effect size[b] (p-FDR)
Cerebellar	Right cerebellum VI (+32 −57 −26)	342	T = −7.92 (<0.001)	Visual and sensorimotor	Right occipital pole (+04 −93 +12)	98	T = −2.94 (0.0052)
	Left cerebellum VI (−23 −57 −21)	336			Right supra calcarine cortex (+17 −82 +18)	22	T = −2.89 (0.0058)
	Left cerebellum IV & V (−11 −49 −20)	170			Right lingual gyrus (+06 −64 +08)	48	
	Vermis VIII (−01 −66 −29)	168					
	Right cerebellum crus 1 (+36 −70 −25)	167					
Visual	Right lingual gyrus (+25 −49 −12)	429	T = −7.92 (<0.001)	Visual and cerebellar	Right intracalcarine cortex (+12 −82 +12)	364	T = −2.64 (0.011)
	Right occipital fusiform gyrus (+25 −78 −16)	235					
	Left lingual gyrus (−15 −60 −03)	225					
	Right occipital pole (+16 −92 +04)	215					
	Left occipital pole (−15 −95 −07)	183					
	Left intracalcarine cortex (−07 −88 +02)	118					
	Right intracalcarine cortex (+08 −89 +01)	108					
Sensorimotor	Left lateral occipital cortex (−21 −68 +57)	831	T = −6.65 (<0.001)				
	Left superior parietal lobule (−26 −66 +58)	172					
	Right postcentral gyrus (+15 −34 +72)	168					
	Left postcentral gyrus (−20 −66 +59)	166					
	Left precentral gyrus (−11 −29 63)	132					

Key: AD, Alzheimer's disease; aMCI, amnestic mild cognitive impairment; HC, cognitively normal healthy controls.

[a] Characterization of each network is derived from the spatial overlap between the CONN network template and the local correlation between-group differences or the independent component (IC) between-group differences.

[b] Effect size refers to the statistical inference derived from the T-value or the size of the difference relative to the variation of the data (i.e., differences in the mean regional activation between groups for a specific region or cluster, for the local correlation analysis, and an independent component for the IC analysis). Multiple t-values correspond to more than one independent cluster within the same network with a high local correlation difference between the compared groups or to multiple regions (i.e., clusters) inside an independent component.
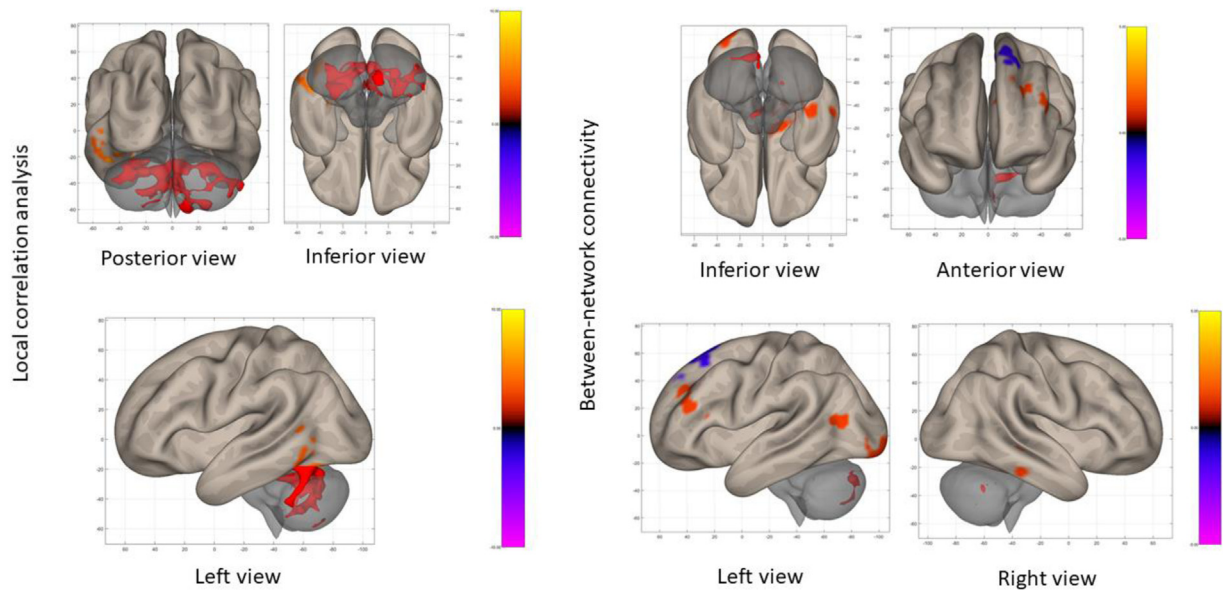
Table 6
Functional connectivity analysis between aMCI with non-AD and with Alzheimer's pathologic change

aMCI with non-AD pathologic change > aMCI with Alzheimer's pathologic change

Local correlation analysis				Between-network connectivity			
Networks[a]	Region (peak activation coordinate)	Cluster size (voxels)	Effect size[b] (p-FDR)	Networks[a]	Region (peak activation coordinate)	Cluster size (voxels)	Effect size[b] (p-FDR)
Cerebellar	Left cerebellum crus 1 (−38 −71 −37)	404	T = 6.41 (<0.001)	Dorsal attention and cerebellar	Left middle frontal gyrus (−25 +36 +32)	181	T = 3.96 (<0.001)
	Right cerebellum VIII (+27 −67 −59)	311			Left cerebellum I (−31 −84 −24)	84	
	Right cerebellum VI (+28 −55 −28)	284			Left inferior frontal gyrus (−43 +33 +16)	47	
	Left cerebellum VI (−38 −71 −25)	275			Left anterior cingulate gyrus (−10 +24 +24)	27	
	Right cerebellum crus 2 (+46 −67 −39)	259					
	Left cerebellum VIII (−15 −63 −46)	247					
	Left cerebellum crus 2 (−16 −59 −47)	180					
	Right cerebellum IX (+11 −67 −47)	180					
Visual	Left inferior temporal gyrus (−44 −44 −11)	167	T = 6.32 (<0.001)	Visual and cerebellar	Left lateral occipital cortex (−46 −69 +10)	217	T = 3.29 (0.0016)
	Left lateral occipital cortex (−49 −62 −18)	78			Left occipital pole (−26 −101 −06)	181	
	Left temporal fusiform cortex (−38 −40 −08)	77			Left cerebellum II (−10 −82 −30)	155	
				Default mode and cerebellar	Right temporal fusiform cortex (+26 −34 −23)	94	T = 2.58 (0.0241)
					Right cerebellum VIII (+15 −76 −51)	76	
				Visual and dorsal attention	Right paracingulate gyrus (+12 −35 +29)	56	T = 2.34 (0.0438)
				Salience and visual	Left frontal pole (−23 +44 +44)	230	T = −2.58 (0.0238)
					Left superior frontal gyrus (−12 +18 +57)	240	

[a] Characterization of each network is derived from the spatial overlap between the CONN network template and the local correlation between-group differences or the independent component (IC) between-group differences.

[b] Effect size refers to the statistical inference derived from the T-value or the size of the difference relative to the variation of the data (i.e., differences in the mean regional activation between groups for a specific region or cluster, for the local correlation analysis, and an independent component for the IC analysis). Multiple t-values correspond to more than one independent cluster within the same network with a high local correlation difference between the compared groups or to multiple regions (i.e., clusters) inside an independent component.

aMCI with non-AD pathologic change > aMCI with AD+ profile

Fig. 5. Functional connectivity analysis between aMCI with non-AD pathologic change and aMCI with Alzheimer's pathologic change. FC, functional connectivity; aMCI, amnestic mild cognitive impairment; AD, Alzheimer's disease. Activation maps are graphical representations of Table 6, where hot colors represent greater mean regional activation (i.e., between clusters for the local correlation analysis and between specific region and independent component for the between-network functional connectivity analysis) in aMCI with non-AD pathologic change than aMCI with Alzheimer's pathologic change, and cold colors represent the opposite contrast or lower mean regional activation (i.e., cold colors reflect the opposite effect, greater mean regional activation in aMCI with Alzheimer's pathologic change than in aMCI with non-AD pathologic change). Subcortical activation is represented in red. Activation values based on T values (i.e., activation color bar range −10 to 10 for the local correlation analysis and −5 to 5 for the between-network connectivity analysis). ICA figures display the cluster within the independent component where the between-group differences are observed and not the connectivity between regions; the color gradients are proportional to the size of the effect (i.e., between-group differences t-values). (For interpretation of the references to color in this figure legend, the reader is referred to the Web version of this article.)

further explored by specifically investigating the differences between prodromal AD (i.e., AD with aMCI) and AD with dementia, which assesses the differences associated with cognitive decline in a population with an explicit pathologic burden compatible with AD (i.e., $A^+T^+(N)^-$ and $A^+T^+(N)^+$ biological profiles). Second, we assessed the effect of cognitive decline on FC in participants with non-AD pathologic change at the initial stages of memory impairment (i.e., cognitively unimpaired participants and aMCI patients). Furthermore, by considering aMCI patients, a sample with stable cognition, the impact of Alzheimer's pathologic change on FC could be assessed by comparing patients with and without Alzheimer's pathologic change. Finally, after defining, comparing, and assessing FC of both clinically (i.e., AD and aMCI) and biologically (i.e., with Alzheimer's pathologic change and with non-AD pathologic change) defined groups, we assessed the neural correlates of

anosognosia in each of the clinically and the biologically characterized cognitively impaired groups studied previously.

4.1. FC related to cognitive decline

Resting-state brain network dysfunction has been previously described in the AD continuum. A study performing network- and voxel-based quantitative meta-analyses on 34 studies reported consistent connectivity alterations in the default mode, salience, and limbic networks in both AD and aMCI patients (Badhwar et al., 2017). The PCC displayed within-network connectivity changes assessed through regional homogeneity and amplitude of low-frequency fluctuations; however, DMN hypoconnectivity in aMCI patients proved to be less (i.e., could only be demonstrated using network-level statistics) than the changes observed in AD patients

Table 7
Simple main effect of anosognosia on the activation and FC in prodromal Alzheimer's disease

Simple main effect of anosognosia						
Group	N	Activation			Functional connectivity	
		Region (peak activation coordinate)	Cluster size (voxels)	Effect size[a] (p-FDR)	Network[b]	Effect size[a] (p-FDR)
Prodromal AD	32	Anterior cingulate gyrus (+18 +28 −10)	704	T= 2.52 (0.043)	1.Visual 2.Default mode 3.Language 4.Cerebellar 5.Sensorimotor	T = 3.72 (<0.001) T = −3.34 (0.0023) T= 3.25 (0.0029) T= −3.20 (0.0033) T= 2.40 (0.0233)

Key: AD, Alzheimer's disease; FC, functional connectivity.
[a] Effect size refers to the statistical inference derived from the T-value or the size of the difference relative to the variation of the data (i.e., variance explained by anosognosia in the mean regional activation and the functional coupling between the anterior cingulate cortex and the different networks).
[b] Characterization of each network is derived from the spatial overlap between the CONN network template and the independent component (IC) between-group differences.

(Badhwar et al., 2017). Furthermore, previous work comparing AD patients to HC observed changes in 3 DMN subnetworks: (1) decreased within-network connectivity in the posterior DMN; (2) increased connectivity in the anterior DMN; and (3) increased connectivity in the ventral DMN (Damoiseaux et al., 2012). Similar changes pointing to both hypo- and hyper-connectivity in the DMN have been observed in aMCI. When compared with HCs, hypo- and hyper-connectivity are observed in aMCI patients (Eyler et al., 2019). Eyler and colleagues (2019), report a meta-analysis of 31 studies where hypoconnectivity in the PCC/precuneus was associated with aMCI; however, when these results were compared with the individual studies, the directionality of the results varied, concluding that the incorporation of biomarker AT(N) classifications "might help to resolve some of the heterogeneity of the DMN findings for MCI" (Eyler et al., 2019; p.115–116). In our study, even after biologically defining prodromal AD, the DMN seems to have connectivity changes pointing to both directions in between-network connectivity but not in within-network FC (i.e., hypo- and hyper-connectivity between networks but not in local correlation analysis).

The DMN is persistently affected independently of the cognitive decline present in the Alzheimer's continuum. When first considering Alzheimer's pathologic change, greater local correlation was observed in the DMN and salience network when comparing aMCI to AD, whereas lower local correlation was seen in the cerebellar and sensorimotor network. Meanwhile, between-network connectivity was increased in the DMN and salience network, whereas between-network connectivity decreased in the cerebellar network in aMCI compared with AD. Local correlation and between-network connectivity comparisons between AD patients and aMCI patients with Alzheimer's pathologic change thus provide insight into brain FC changes during a cognitive decline transitional stage (i.e., cognitive impairment to dementia) in the Alzheimer's continuum. Similar to our findings, the DMN and the salience network have been shown to be disrupted in aMCI and AD patients. Although the patients were not classified according to AT(N) profile, recent PET/ MRI data from AD patients suggest a disruption in the DMN signaling pathways; furthermore, neuronal injury was identified as FDG PET hypometabolism in subnetwork regions of the DMN, the parietal cortices, and hippocampus (Scherr et al., 2019). Regarding the association of cognitive decline (i.e., decreased cognitive performance in MoCA) and the degree of network disruption in aMCI, the salience network is primarily affected (Chand et al., 2015).

Prodromal AD has the highest rate of short-term clinical progression to dementia, and AD with dementia has the most precise biological and clinical characterization among the different stages of the in vivo classification of AD-associated cognitive deterioration. Therefore, studying the brain network differences between prodromal AD and AD with dementia allows for a more in-depth understanding of the transitional stage from aMCI into AD in the AD continuum. When the biological classification was narrowed so that only cognitively impaired participants with Alzheimer's compatible pathologic disease burden were compared, we found that the DMN showed increased, and the cerebellar and somatosensory networks decreased local correlation in aMCI with Alzheimer's pathologic change compared with AD. Others, Brier et al. (2012) and Hafkemeijer et al. (2012), found that both within-network (comparable to local correlation) and between-network FC are decreased between the anterior and posterior portion of the DMN in the early stages of AD (Brier et al., 2012; Hafkemeijer et al., 2012).

FC analytic approaches can be divided into functional segregation measures (e.g., integrated local correlation) and functional integration approaches (e.g., ICA) (Lv et al., 2018). Local correlation analysis provides insight into the local function of specific brain regions or "within-network connectivity"; meanwhile, ICAs focus

on the functional relationship between different brain areas or "between-network connectivity." In this study, we used local correlation as a measure of functional segregation, focusing on the local function of specific brain regions; thus, within-network FC can be interpreted (Deshpande et al., 2009). As a voxel-to-voxel measure of functional integration, we used ICA, which is a straightforward measure of between-network FC (Wylie et al., 2015). For a didactic explanation of within-network and between-network FC analytical approaches across different fMRI statistical analyses, we refer the reader to the review by Lv et al. (2018). Changes in local correlation and between-network connectivity because of non- –AD-associated cognitive deterioration were also assessed by comparing cognitively unimpaired participants and aMCI patients with non-AD pathologic change. Cognitive decline (i.e., aMCI > HC) in non-AD pathologic disease burden is associated with higher local correlation in the cerebellar, visual, and sensorimotor networks and greater between-network connectivity of the visual network with both the sensorimotor and cerebellar networks. To the best of our knowledge, there is no information about FC differences between cognitively unimpaired participants and aMCI patients with non-AD pathologic changes. Although our work assesses patients with cognitive decline and AT(N) profiles cross-sectionally, recently, a study of ATN classification and cognitive decline in patients with subjective cognitive decline (i.e., cognitively unimpaired patients with memory complaints) showed that patients with biomarker profiles associated with both non-AD (i.e., $A^-T^+N^+$) and Alzheimer's pathologic changes (i.e., $A^+T^-N^-$, $A^+T^+N^-$, $A^+T^-N^+$, and $A^+T^+N^+$) were at increased risk of dementia. However, the presence of amyloid burden (i.e., A^+ profile) was associated with steeper memory, attention, language, and executive function decline (Ebenau et al., 2020). Our findings and the finding from Ebenau et al. (2020) support the hypothesis that patients with AT(N) biomarker profiles with Alzheimer's pathologic changes are at higher risk of developing cognitive and functional changes compatible with AD. In our study, we observed that the cerebellar network was linked with reduced FC (i.e., local correlation and between-network) in association with non-AD pathologic changes. FC changes within and between the cerebellar network have not been reported; however, cerebellar volume may contribute to the cognition level in an early stage of the Alzheimer's disease continuum (Lin et al., 2020). Functional changes might precede structural changes in the cerebellum early in the Alzheimer's disease continuum. We observed that FC changes in the cerebellar network are associated with non-AD pathologic changes in aMCI. The cerebellar network had lower local correlation and between-network connectivity in aMCI than cognitively unimpaired participants with non-AD pathologic change and higher local correlation and between-network connectivity in aMCI with non-AD pathologic change than aMCI with Alzheimer's pathologic change. All in all, changes in resting-state brain FC observed in the cerebellum might serve as early signs not only of structural changes but also of non-AD pathologic changes early in the Alzheimer's disease continuum.

4.2. FC related to biological disease burden

To the best of our knowledge, this is the first report that assesses FC differences between aMCI patients with Alzheimer's pathologic change and those with non-AD pathologic change. Comparing the local correlation and between-network connectivity of aMCI patients with non-AD pathologic change to aMCI patients with Alzheimer's pathologic change biological profiles provides information about the role of disease burden in FC in a population at risk of developing dementia (i.e., aMCI). In this group, non-AD pathologic change was associated with higher local correlation in the visual and cerebellar networks and higher between-network connectivity

Effect of anosognosia in prodromal Alzheimer's disease

Left medial view

Right medial view
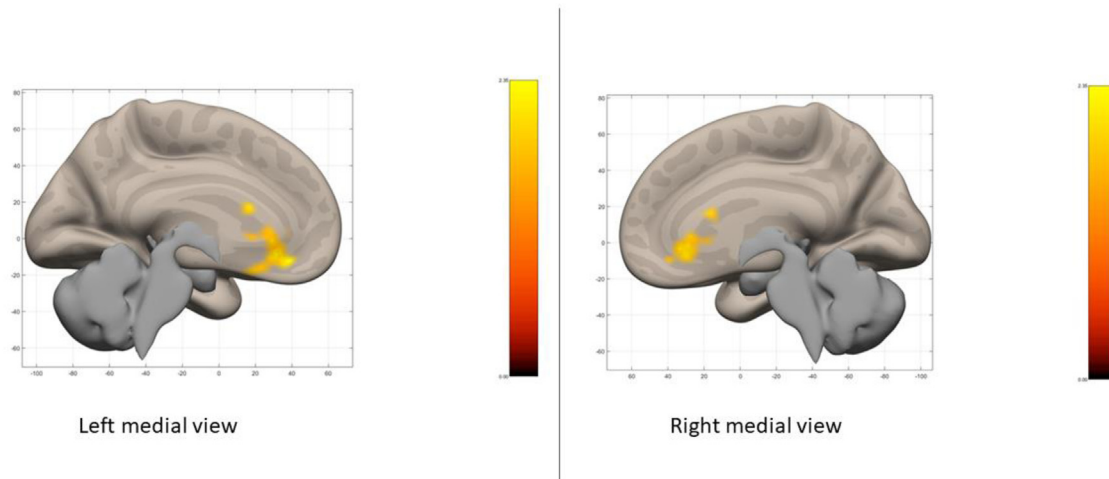
Fig. 6. Voxel-wise regression analysis of anosognosia in prodromal AD. Activation maps are graphical representations of Table 7, where hot colors represent the simple main effect of anosognosia in the variance of the mean regional activation. Activation values based on t-values (i.e., activation color bar range 0–2.7). (For interpretation of the references to color in this figure legend, the reader is referred to the Web version of this article.)

primarily in the visual, cerebellar, and dorsal attention network. Alzheimer's pathologic change in this group was associated with higher between-network connectivity between the salience and visual network These results are in line with the association previously described between cognitively unimpaired participants and aMCI patients with non-AD pathologic changes, where the cerebellar network as well as the visual network could be altered early in a non-AD disease continuum.

4.3. Neural correlates of anosognosia in prodromal AD

The secondary objective of this study was to evaluate if anosognosia was a contributing factor that might explain the previously assessed between-group differences; with this in mind, we explored the neural correlates associated with anosognosia in AD and aMCI patients included in this study (i.e., clinical AD, prodromal AD, aMCI with non-AD pathologic change, and AD with dementia). Between-group comparisons showed reduced within- and between-network connectivity in the DMN regions of AD patients with anosognosia compared with AD patients without anosognosia and controls (Mondragón et al., 2019) and reduced between-network FC between the DMN and the insular cortex (Berlingeri et al., 2015). A disconnection within and between DMN memory subsystems was related to increased anosognosia discrepancy scores in patients with AD (Antoine et al., 2019). Anosognosia in aMCI patients was associated with reduced FC between the precuneus and the bilateral inferior parietal lobes, left PCC, and left orbitofrontal cortex, as well as between the right hippocampus and left middle temporal lobe and right fusiform cortex (Vannini et al., 2017). Our results point to the ACC as the brain region related to anosognosia in prodromal AD. Through a voxel-vise regression analysis, we found that brain connectivity in the ACC was positively associated with anosognosia in prodromal AD patients. The ACC is a major hub of the salience network with a key role in processing and integrating internal and external inputs for decision-making (Seeley et al., 2007). Reduced gray matter density, cerebral blood flow, and hypometabolism in the inferior frontal gyrus, ACC, and medial temporal lobe have been associated with increased anosognosia of memory deficits in AD (Hallaman et al., 2020). Bilateral ACC volume reduction, among other regions (i.e., lingual gyrus, fusiform gyrus, and thalamus), has also been associated with

anosognosia of memory deficits in early-AD patients (Varela-Bermejo et al., 2020). The dorsal or pregenual ACC (pACC) cluster was predominantly associated with anosognosia in the prodromal AD patients in this study. The pACC is a major hub in the ventral salience network and is highly connected with paralimbic regions, subcortical and brainstem structures, as well as frontoparietal regions (Tourgoutoglou and Dickerson, 2019). The pACC along with the anterior midcingulate cortex is a core location of neurodegeneration early during frontotemporal dementia (FTD); furthermore, the PCC has been related to impaired awareness of autobiographical memory (Tourgoutoglou and Dickerson, 2019).

4.4. Limitations and future perspectives

Although the ECog composite score (i.e., discrepancy score between the patient's and caregiver's score) has been previously used to assess anosognosia in the ADNI cohort. However, the ECog scale was not designed for this purpose and could be underrepresenting anosognosia in this cohort; thus, explaining why the effect of this behavioral variable is only observed in the most biologically specific comparison (i.e., prodromal AD versus AD with dementia). Studies that incorporate the AT(N) classification and use a specific awareness of memory deficit scale or diagnose anosognosia through a clinical consensus are therefore needed. In this study, we used a biological approach and definition to explore FC between-group differences; thus, the neuropsychological test battery reported is not comprehensive, and only clinical group averages are reported. We only included a neuropsychological test that assesses global function, limiting the interpretation of between-group differences. However, the aim of this study was not to assess domain-specific changes, as task-based fMRI paradigms are better suited to underpin neuropsychological changes than resting-state recordings. Future studies should explore the association between specific cognitive domains and between-group FC differences in AT(N) defined groups using task-based paradigms.

We based our AT(N) cutoff values on previously established thresholds for the ADNI cohort; however, the use of cutoff values could have led to a loss of information, especially pertaining to amyloid burden as subthreshold amyloid accumulation could represent the earliest detectable indication of pathology (Landau et al., 2018). Future studies with large AT(N) subgroups could

consider using biomarkers as continuous variables to avoid losing information associated with the use of dichotomized biomarker data. Furthermore, of the 26 cognitively unimpaired participants included, none were truly HC participants (i.e., 6 with AD pathologic changes and 20 with non-AD pathologic changes). This finding raises the question about how "truly healthy" the control participants are. Before the use of the NIA-AA research framework, studies only used cognitive scores to designate control participants. Future studies should consider recruiting and including AT(N) negative cognitively unimpaired participants as their HCs. In addition, ADNI participants are highly educated and are self-aware of their cognitive abilities; thus, they are considered a convenience sample. In cognitively unimpaired ADNI participants, cognitive reserve (i.e., the capacity to withstand pathologic disease burden; hence, accounting for individual differences in the susceptibility to age-related brain changes or AD-related pathology) could be a contributing factor to the normal cognitive performance in participants with AD and non-AD pathologic changes in this study.

Resting-state brain connectivity has certain limitations. It should be noted that the results reported here assess resting-state fMRI data, which provide insight into the effect size of between-group differences in FC but not into their relationship with task-based performance. The results presented previously show a lack of distinct directionality in 2 between-group comparisons (this concerns ICA between-group differences among prodromal AD and AD with dementia as well as FC between the sensorimotor network and the DMN and between the cerebellar network and the DMN). The lack of directionality might be a reflection of the complexity in the functional brain network dynamics associated with the changes related to cognitive deterioration or simply a reflection of the outcome measure's strength (or lack) of association, a limitation often related to resting-state fMRI paradigms. We believe the first to be true: our main conclusion is, as changes are observed in both directions in the between-network FC, this is evidence for loss of network integrity. However, more studies are needed to assess the small between-group differences found in AT(N) defined groups with task-based paradigms; this is especially true in assessing the FC of the salience, dorsal attention, and sensorimotor network. The limited scope of resting-state fMRI does not allow for the adequate assessment of memory, attention, language, and executive function processes; task-based fMRI studies are necessary to understand changes in these cognitive domains. Task-based fMRI studies are necessary to assess the role of the salience, dorsal attention, somatosensory networks, as resting-state fMRI studies do not provide concluding evidence regarding the alterations found between groups in the Alzheimer and non-AD disease continuum. Another limitation of this study is the unbalanced number of participants included in the group comparisons. We decided to keep all available participants rather than perform balanced group comparisons. Unbalanced designs in fMRI studies can be an issue as the sample-sizes dwindles. There exists no clear guidance regarding containing interactions within the framework of the GLM in unbalanced neuroimaging data sets (McFarquhar, 2016). Smaller groups have a larger margin of error (i.e., larger standard of error for a regression coefficient) because of its smaller sample size even if the within-group SDs are the same across the compared groups. Although overparameterized ANOVA models in the GLM are possible and implementable in SPM (McFarquhar, 2016), we chose to perform conjunction analyses to correct for having unbalanced groups. Conjunction analyses using different contrasts are possible in the CONN toolbox and are described in the Methods section (Friston et al., 1999), *vide supra*; however, this correction does not prevent heteroscedasticity in the GLM model or the homogeneity of variances assumption in a two-sample *t*-test, which should be assessed in the imaging preprocessing quality assessment phase. Although we corrected for unbalanced group sizes, these procedures in neuroimaging

are still a topic of debate. Furthermore, on October 28, 2020, a search on the ADNI-3 database was performed, yielding 61 AD patients with fMRI imaging. Yet, for this study, we chose not to include ADNI-3 imaging data, because at the time these data were extracted, few participants had available information; we recommend that future studies should compare between-group differences among ADNI-2 and ADNI-3 datasets, as well as explore AD patient differences using larger groups.

4.5. Conclusion

Using biological definitions, the DMN connectivity is persistently affected in the early stages of the Alzheimer's biological continuum, which is on par with findings from clinically defined groups in the AD continuum. Furthermore, the non-AD pathologic burden is related to visual and cerebellar network connectivity changes. FC of the ACC is associated with anosognosia in prodromal AD; thus, between-network connectivity changes in the ACC might precede changes found in the PCC, a DMN region typically associated in AD with anosognosia. The results presented here add to the supporting evidence that proposes the DMN and the ACC as key hubs associated with cognitive decline in the AD continuum and anosognosia, respectively; this network and region could serve in the future as ROI to monitor brain connectivity changes associated with prodromal AD and awareness of memory deficits.

Disclosure statement

Acknowledgements

Appendix A. Supplementary data

References (Alzheimer's Disease Neuroimaging, 2010) and (Martuzzi et al., 2011) are cited in the Appendix.

Supplementary data to this article can be found online at https://doi.org/10.1016/j.neurobiolaging.2020.12.021.

References

Alzheimer's Disease Neuroimaging I, 2010. ADNI general procedures manual. http://adni.loni.usc.edu/methods/documents/. (Accessed 15 November 2018).

Antoine, N., Bahri, M.A., Bastin, C., Collette, F., Phillips, C., Balteau, E., Genon, S., Salmon, E., 2019. Anosognosia and default mode subnetwork dysfunction in Alzheimer's disease. Hum. Brain Mapp. 40, 5330−5340.

Ashburner, J., 2007. A fast diffeomorphic image registration algorithm. Neuroimage 38, 95−113.

Badhwar, A., Tam, A., Dansereau, C., Orban, P., Hoffstaedter, F., Bellec, P., 2017. Resting-state network dysfunction in Alzheimer's disease: a systematic review and meta-analysis. Alzheimers Dement (Amst). 8, 73−85.

Berlingeri, M., Ravasio, A., Cranna, S., Basilico, S., Sberna, M., Bottini, G., Paulesu, E., 2015. Unrealistic representations of "the self": a cognitive neuroscience assessment of anosognosia for memory deficit. Conscious Cogn. 37, 160−177.

Brier, M.R., Thomas, J.B., Snyder, A.Z., Benzinger, T.L., Zhang, D., Raichle, M.E., Holtzman, D.M., Morris, J.C., Ances, B.M., 2012. Loss of intranetwork and internetwork resting state functional connections with Alzheimer's disease progression. J. Neurosci. 32, 8890−8899.

Calhoun, V.D., Adali, T., Pearlson, G.D., Pekar, J.J., 2001. A method for making group inferences from functional MRI data using independent component analysis. Hum. Brain Mapp. 14, 140−151.

Castrillo Sanz, A., Andrés Calvo, M., Repiso Gento, I., Izquierdo Delgado, E., Gutierrez Ríos, R., Rodríguez Herrero, R., Rodríguez Sanz, F., Tola-Arribas, M.A., 2016.

Anosognosia in Alzheimer disease: prevalence, associated factors, and influence on disease progression. Neurologia 31, 296–304.

Chand, G.B., Wu, J., Hajjar, I., Qiu, D., 2015. Interactions of the salience network and its subsystems with the default-mode and the central-executive networks in normal aging and mild cognitive impairment. Brain connect. Dowling NM, Johnson SC, Gleason CE, Jagust WJ; Alzheimer's disease neuroimaging initiative. The mediational effects of FDG hypometabolism on the association between cerebrospinal fluid biomarkers and neurocognitive function. Neuroimage 105, 357–368.

Damoiseaux, J.S., Prater, K.E., Miller, B.L., Greicius, M.D., 2012. Functional connectivity tracks clinical deterioration in Alzheimer's disease. Neurobiol. Aging 33, 828.e19-828.e8.28E30.

Deshpande, G., LaConte, S., Peltier, S., Hu, X., 2009. Integrated local correlation: a new measure of local coherence in fMRI data. Hum. Brain Mapp. 30, 13–23.

Dowling, N.M., Johnson, S.C., Gleason, C.E., Jagust, W.J., 2015. Alzheimer's Disease Neuroimaging Initiative. The mediational effects of FDG hypometabolism on the association between cerebrospinal fluid biomarkers and neurocognitive function. Neuroimage 105, 357–368.

Dubois, B., Feldman, H.H., Jacova, C., Hampel, H., Molinuevo, J.L., Blennow, K., DeKosky, S.T., Gauthier, S., Selkoe, D., Bateman, R., Cappa, S., Crutch, S., Engelborghs, S., Frisoni, G.B., Fox, N.C., Galasko, D., Habert, M.O., Jicha, G.A., Nordberg, A., Pasquier, F., Rabinovici, G., Robert, P., Rowe, C., Salloway, S., Sarazin, M., Epelbaum, S., de Souza, L.C., Vellas, B., Visser, P.J., Schneider, L., Stern, Y., Scheltens, P., Cummings, J.L., 2014. Advancing research diagnostic criteria for Alzheimer's disease: the IWG-2 criteria. Lancet Neurol. 13, 614–629.

Ebenau, J.L., Timmers, T., Wesselman, L.M.P., Verberk, I.M.W., Verfaillie, S.C.J., Slot, R.E.R., van Harten, A.C., Teunissen, C.E., Barkhof, F., van den Bosch, K.A., van Leeuwenstijn, M., Tomassen, J., Braber, A.D., Visser, P.J., Prins, N.D., Sikkes, S.A.M., Scheltens, P., van Berckel, B.N.M., van der Flier, W.M., 2020. ATN classification and clinical progression in subjective cognitive decline: The SCIENCe Project. Neurology 95, e46–e58.

Eyler, L.T., Elman, J.A., Hatton, S.N., 2019. Resting state abnormalities of the default mode network in mild cognitive impairment: a systematic review and meta-analysis. J. Alzheimers Dis. 70, 107–120.

Farias, S.T., Mungas, D., Reed, B.R., Cahn-Weiner, D., Jagust, W., Baynes, K., Decarli, C., 2008. The measurement of everyday cognition (ECog): scale development and psychometric properties. Neuropsychology 22, 531–544.

Friston, K.J., Holmes, A.P., Price, C.J., Büchel, C., Worsley, K.J., 1999. Multisubject fMRI studies and conjunction analyses. Neuroimage 10, 385–396.

Gerretsen, P., Chung, J.K., Shah, P., Plitman, E., Iwata, Y., Caravaggio, F., Nakajima, S., Pollock, B.G., Graff-Guerrero, A., Alzheimer's Disease Neuroimaging Initiative, 2017. Anosognosia is an independent predictor of conversion from mild cognitive impairment to Alzheimer's disease and is associated with reduced brain metabolism. J. Clin. Psychiatry 78, e1187–e1196.

Hafkemeijer, A., van der Grond, J., Rombouts, S.A., 2012. Imaging the default mode network in aging and dementia. Biochim. Biophys. Acta 1822, 431–441.

Hallam, B., Chan, J., Gonzalez Costafreda, S., Bhome, R., Huntley, J., 2020. What are the neural correlates of meta-cognition and anosognosia in Alzheimer's disease? A systematic review [published online ahead of print, 2020 Jun 18]. Neurobiol. Aging 94, 250–264.

Jack Jr., C.R., Bennett, D.A., Blennow, K., Carrillo, M.C., Dunn, B., Haeberlein, S.B., Holtzman, D.M., Jagust, W., Jessen, F., Karlawish, J., Liu, E., Molinuevo, J.L., Montine, T., Phelps, C., Rankin, K.P., Rowe, C.C., Scheltens, P., Siemers, E., Snyder, H.M., Sperling, R., Contributors, 2018. NIA-AA Research Framework: toward a biological definition of Alzheimer's disease. Alzheimers Dement. 14, 535–562.

Jagust, W.J., Landau, S.M., Koeppe, R.A., Reiman, E.M., Chen, K., Mathis, C.A., Price, J.C., Foster, N.L., Wang, A.Y., 2015. The Alzheimer's disease neuroimaging initiative 2 PET core: 2015. Alzheimers Dement 11, 757–771.

Landau, S.M., Breault, C., Joshi, A.D., Pontecorvo, M., Mathis, C.A., Jagust, W.J., Mintun, M.A., Alzheimer's Disease Neuroimaging Initiative, 2013. Amyloid-β imaging with Pittsburgh compound B and florbetapir: comparing radiotracers and quantification methods. J. Nucl. Med. 54, 70–77.

Landau, S.M., Horng, A., Jagust, W.J., 2018. Alzheimer's Disease Neuroimaging Initiative. Memory decline accompanies subthreshold amyloid accumulation. Neurology 90, e1452–e1460.

Langer, K.G., Levine, D.N., 2014. Babinski, J. (1914). Contribution to the study of the mental disorders in hemiplegia of organic cerebral origin (anosognosia). Translated by K.G. Langer & D.N. Levine. Translated from the original Contribution à l'Étude des Troubles Mentaux dans l'Hémiplégie Organique Cérébrale (Anosognosie). Cortex 61, 5–8.

Lin, C.Y., Chen, C.H., Tom, S.E., Kuo, S.H., Alzheimer's Disease Neuroimaging Initiative, 2020. Cerebellar volume is associated with cognitive decline in mild cognitive impairment: results from ADNI. Cerebellum 19, 217–225.

Lv, H., Wang, Z., Tong, E., Williams, L.M., Zaharchuk, G., Zeineh, M., Goldstein-Piekarski, A.N., Ball, T.M., Liao, C., Wintermark, M., 2018. Resting-state functional MRI: everything that nonexperts have always wanted to know. AJNR Am. J. Neuroradiol 39, 1390–1399.

Martuzzi, R., Ramani, R., Qiu, M., Shen, X., Papademetris, X., Constable, R.T., 2011. A whole-brain voxel based measure of intrinsic connectivity contrast reveals local changes in tissue connectivity with anesthetic without a priori assumptions on thresholds or regions of interest. Neuroimage 58, 1044–1050.

McFarquhar, M., 2016. Testable hypotheses for unbalanced neuroimaging data. Front Neurosci. 10, 270.

McKhann, G., Drachman, D., Folstein, M., Katzman, R., Price, D., Stadlan, E.M., 1984. Clinical diagnosis of Alzheimer's disease: report of the NINCDS-ADRDA work group under the auspices of department of health and human services task force on Alzheimer's disease. Neurology 34, 939–944.

Mondragón, J.D., Maurits, N.M., De Deyn, P.P., 2019. Functional neural correlates of anosognosia in mild cognitive impairment and Alzheimer's disease: a systematic review. Neuropsychol. Rev. 29, 139–165.

Mueller, S.G., Weiner, M.W., Thal, L.J., Petersen, R.C., Jack, C.R., Jagust, W., Trojanowski, J.Q., Toga, A.W., Beckett, L., 2005. Ways toward an early diagnosis in Alzheimer's disease: the Alzheimer's disease neuroimaging initiative (ADNI). Alzheimers Dement 1, 55–66.

O'Bryant, S.E., Waring, S.C., Cullum, C.M., Hall, J., Lacritz, L., Massman, P.J., Lupo, P.J., Reisch, J.S., Doody, R., Texas Alzheimer's Research Consortium, 2008. Staging dementia using clinical dementia rating scale sum of boxes scores: a Texas Alzheimer's research consortium study. Arch. Neurol. 65, 1091–1095.

Petersen, R.C., 2004. Mild cognitive impairment as a diagnostic entity. J. Intern. Med. 256, 183–194.

Scherr, M., Utz, L., Tahmasian, M., Pasquini, L., Grothe, M.J., Rauschecker, J.P., Grimmer, T., Drzezga, A., Sorg, C., Riedl, V., 2019. Effective connectivity in the default mode network is distinctively disrupted in Alzheimer's disease-A simultaneous resting-state FDG-PET/fMRI study. Hum. Brain Mapp.

Seeley, W.W., Menon, V., Schatzberg, A.F., Keller, J., Glover, G.H., Kenna, H., Reiss, A.L., Greicius, M.D., 2007. Dissociable intrinsic connectivity networks for salience processing and executive control. J. Neurosci. 27, 2349–2356.

Shaw, L.M., Vanderstichele, H., Knapik-Czajka, M., Clark, C.M., Aisen, P.S., Petersen, R.C., Blennow, K., Soares, H., Simon, A., Lewczuk, P., Dean, R., Siemers, E., Potter, W., Lee, V.M., Trojanowski, J.Q., 2009. Alzheimer's Disease Neuroimaging Initiative. Cerebrospinal fluid biomarker signature in Alzheimer's disease neuroimaging initiative subjects. Ann. Neurol. 65, 403–413.

Shaw, L.M., Vanderstichele, H., Knapik-Czajka, M., Figurski, M., Coart, E., Blennow, K., Soares, H., Simon, A.J., Lewczuk, P., Dean, R.A., Siemers, E., Potter, W., Lee, V.M.Y., Trojanowski, J.Q., 2011. Alzheimer's Disease Neuroimaging Initiative. Qualification of the analytical and clinical performance of CSF biomarker analyses in ADNI. Acta Neuropathol. 121, 597–609.

Sperling, R.A., Aisen, P.S., Beckett, L.A., Bennett, D.A., Craft, S., Fagan, A.M., Iwatsubo, T., Jack Jr., C.R., Kaye, J., Montine, T.J., Park, D.C., Reiman, E.M., Rowe, C.C., Siemers, E., Stern, Y., Yaffe, K., Carrillo, M.C., Thies, B., Morrison-Bogorad, M., Wagster, M.V., Phelps, C.H., 2011. Toward defining the preclinical stages of Alzheimer's disease: recommendations from the National Institute on Aging-Alzheimer's Association workgroups on diagnostic guidelines for Alzheimer's disease. Alzheimers Dement 7, 280–292.

Starkstein, S.E., 2014. Anosognosia in Alzheimer's disease: diagnosis, frequency, mechanism and clinical correlates. Cortex 61, 64–73.

Starkstein, S.E., Brockman, S., Bruce, D., Petracca, G., 2010. Anosognosia is a significant predictor of apathy in Alzheimer's disease. J. Neuropsychiatry Clin. Neurosci. 22, 378–383.

Stephan, K.E., Friston, K.J., 2009. Functional connectivity. Encyclopedia Neurosci. 391–397.

Turró-Garriga, O., Garre-Olmo, J., Calvó-Perxas, L., Reñé-Ramírez, R., Gascón-Bayarri, J., Conde-Sala, J.L., 2016. Course and determinants of anosognosia in Alzheimer's disease: a 12-month follow-up. J. Alzheimers Dis. 51, 357–366.

Touroutoglou, A., Dickerson, B.C., 2019. Cingulate-centered large-scale networks: normal functions, aging, and neurodegenerative disease. Handb. Clin. Neurol. 166, 113–127.

Vannini, P., Hanseeuw, B., Munro, C.E., Amariglio, R.E., Marshall, G.A., Rentz, D.M., Pascual-Leone, A., Johnson, K.A., Sperling, R.A., 2017. Anosognosia for memory deficits in mild cognitive impairment: insight into the neural mechanism using functional and molecular imaging. Neuroimage Clin. 15, 408–414.

Valera-Bermejo, J.M., De Marco, M., Mitolo, M., McGeown, W.J., Venneri, A., 2020. Neuroanatomical and cognitive correlates of domain-specific anosognosia in early Alzheimer's disease [published online ahead of print, 2020 May 14]. Cortex 129, 236–246.

White, T., Calhoun, V.D., 2019. Dissecting static and dynamic functional connectivity: example from the autism spectrum. J. Exp. Neurosci. 13, 1179069519851809.

Whitfield-Gabrieli, S., Nieto-Castanon, A., 2012. Conn: a functional connectivity toolbox for correlated and anticorrelated brain networks. Brain Connect. 2, 125–141.

Wylie, K.P., Kronberg, E., Maharajh, K., Smucny, J., Cornier, M.A., Tregellas, J.R., 2015. Between-network connectivity occurs in brain regions lacking layer IV input. Neuroimage 116, 50–58.